

COMPUTATIONAL METHODS FOR DESIGN OF
SMART MATERIAL MORPHING STRUCTURES
WITH LOCALIZED ACTIVATION AND
ACTUATION

by

Shuang Wang

BS in Water Conservancy and Hydropower Engineering, Wuhan
University, China, 2009

MS in Structural Engineering and Mechanics, University of
Pittsburgh, U.S., 2011

Submitted to the Graduate Faculty of
the Swanson School of Engineering in partial fulfillment
of the requirements for the degree of
Doctor of Philosophy

University of Pittsburgh

2014

UNIVERSITY OF PITTSBURGH
SWANSON SCHOOL OF ENGINEERING

This dissertation was presented

by

Shuang Wang

It was defended on

August 22nd, 2014

and approved by

John C. Brigham, PhD, Assistant Professor, Department of Civil and Environmental
Engineering and Bioengineering

Jeen-Shang Lin, ScD, Associate Professor, Department of Civil and Environmental
Engineering

Qiang Yu, PhD, Assistant Professor, Department of Civil and Environmental Engineering

Richard Beblo, PhD, Research Engineer, University of Dayton Research Institute

Dissertation Director: John C. Brigham, PhD, Assistant Professor, Department of Civil
and Environmental Engineering and Bioengineering

Copyright © by Shuang Wang

2014

COMPUTATIONAL METHODS FOR DESIGN OF SMART MATERIAL MORPHING STRUCTURES WITH LOCALIZED ACTIVATION AND ACTUATION

Shuang Wang, PhD

University of Pittsburgh, 2014

There is significant ongoing interest to develop smart structure technologies, such as those that can automatically detect their condition and/or actively change their geometry or material behaviors to adapt to adverse conditions or otherwise improve operational efficiency. Of the structural materials under development for smart structure applications, active smart materials are attracting increasing attentions due to their abilities to exhibit controlled variable stiffness through activation (e.g., thermal, electrical, or light activation) and experience extremely large deformations and shape changes without damage. Active smart materials, such as shape memory polymers, are currently being explored and show promise as morphing skins, replacements to mechanical hinges, and other structural components. Moreover, in a general sense any structure or structural component that is fully composed of active smart materials could have limitless shape-changing functionality if provided sufficient activation and actuation. Towards the design or control of smart structures to utilize such functionality, it is of paramount importance to develop strategies to efficiently solve the coupled multi-physics inverse problems of identifying the optimal activation stimulus and mechanical actuation to achieve desired morphing processes.

The objective of the present work is to develop and investigate a computational strategy for computationally efficient estimation of the parameters relating to the distribution and sequencing of activation and actuation for a morphing smart material structure or structural component to efficiently and effectively achieve a desired morphing function. This strategy

combines a numerical representation of the morphing process with an optimization algorithm to estimate the activation and actuation parameters that best address cost functions and constraints relating to energy consumption, target shape change(s), morphing time, and/or damage prevention. In particular, the strategy is presented in the context of morphing structures or structural components composed of thermally responsive smart materials, and with specific properties based on thermally responsive shape memory polymers.

First, as a proof of concept, an initial computational framework is presented which combines a numerical representation of linear thermo-mechanical behavior of conceptual smart material structures with a non-gradient based optimization technique to identify the activation and actuation parameters to achieve the desired morphing process. The computational inverse mechanics approach is shown through numerical tests to provide a generalized and flexible means to facilitate the use of smart material structures to achieve desired morphing processes with controllable localized activation and actuation. Towards improving the computational efficiency, a variation of the computational framework based on a gradient-based optimization algorithm using the adjoint method is then presented. Numerical examples are shown to verify and test the computational approach, in which the synchronization of multiple activation and actuation parameters is optimized with respect to the energy cost and target shape changes in morphing skeletal structural components. The computational design approach with the adjoint method is shown to provide the capability to efficiently identify activation and actuation parameters to achieve desired morphing capabilities. Moreover, the computational approach is shown to be capable of determining energy-efficient design solutions for a diverse set of target shape changes with fixed instrumentation, providing the potential for substantial functionality beyond what could be expected through traditional empirical design strategies. Finally, to establish the theories and implementation aspects that would be applicable to a variety of structural behaviors, material types and morphing concepts, the efficient computational framework using the adjoint method is generalized to be applicable to various thermally-responsive smart materials. Numerical tests are shown to verify the generalized computational framework, in which the synchronization of multiple activation and actuation parameters is optimized with respect to energy cost and target shape changes in morphing structures with nonlinear thermo-mechanical behaviors (rather

than the purely linear behaviors considered previously). In addition, the significant influence of the nonlinearity in the thermal modeling on the morphing processes, and ultimately the design solutions is explored.

TABLE OF CONTENTS

PREFACE	xiv
1.0 A COMPUTATIONAL FRAMEWORK FOR THE OPTIMAL DESIGN OF MORPHING PROCESSES IN LOCALLY ACTIVATED SMART MATERIAL STRUCTURES	1
1.1 Abstract	1
1.2 Introduction	2
1.3 Computational Design Framework	4
1.4 Numerical Investigation of Optimal Design Problem	9
1.4.1 Forward Problem	10
1.4.2 Optimization Algorithm	12
1.4.3 Example 1: Smart Link	14
1.4.3.1 Sensitivity Analysis:	17
1.4.3.2 Optimization Problem:	19
1.4.3.3 Optimization Results and Discussion:	20
1.4.4 Example 2: Morphing Structural Backbone	26
1.4.4.1 Optimization Problem:	28
1.4.4.2 Optimization Results:	28
1.5 Conclusion	29
2.0 A COMPUTATIONALLY EFFICIENT APPROACH FOR OPTIMAL DESIGN OF SMART MATERIAL MORPHING STRUCTURES USING THE ADJOINT METHOD	33
2.1 Abstract	33

2.2	Introduction	34
2.3	Computational Design/Control Framework for Morphing Structures	38
2.4	Forward Problem	39
2.5	Optimization Objectives and Solution Algorithm	42
2.5.1	Gradient Calculation using the Adjoint Method	43
2.6	Numerical Investigation	46
2.6.1	Example 1: Smart Link	47
2.6.1.1	Results and Discussion:	50
2.6.2	Example 2: Morphing Structural Backbone	52
2.6.2.1	Results and Discussion:	55
2.7	Conclusions	58
3.0	A COMPUTATIONAL INVESTIGATION OF THE EFFECTS OF NONLINEAR THERMAL BEHAVIOR ON THE DESIGN OF LOCALLY ACTIVATED THERMALLY RESPONSIVE SMART MATERIAL MORPHING STRUCTURES	60
3.1	Abstract	60
3.2	Introduction	61
3.3	Computational Design Approach for Locally Activated Morphing Structures	63
3.4	Forward Prediction of Morphing Structure Behavior	64
3.5	Gradient-Based Optimization using Adjoint Method	66
3.6	Numerical Investigation	70
3.6.1	Example 1: Morphing Structural Backbone	70
3.6.1.1	Results and Discussion:	73
3.6.2	Example 2: Morphing Airfoil Structures	76
3.6.2.1	Results and Discussion:	78
3.7	Conclusions	81
4.0	CURRENT CAPABILITIES AND FUTURE DIRECTIONS	82
	BIBLIOGRAPHY	84

LIST OF TABLES

1.1	Assumed material parameters for the numerical study.	13
1.2	Applied displacement boundary conditions for Example 1: Smart Link.	16
1.3	Relative (percent) change in total energy to complete the morph for changes of 20% and 40% for each potential design variable, respectively, for the elliptic path and angle of deformation $\theta = \pi/4 rad$ for Example 1: Smart Link.	18
1.4	Summary of the optimization problem and solution approach for Example 1: Smart Link.	19
1.5	Control and optimized (Opt) design parameters and resulting energy consumption to perform the morph and percent difference (%Diff) with respect to the control design for two angles of deformation with the elliptic path of deformation for Example 1: Smart Link ($\sigma_{tre}^{max} = \ \sigma^{tresca}\ _{L_\infty(\Omega)}$, $mJ = 10^{-3} Joule$).	21
1.6	Control and optimized (Opt) design solutions, resulting temperature distribution at initiation of morphing, and Tresca stress distribution and deformed shape at completion of morphing for angle of deformation $\pi/4 rad$ with the elliptic path of deformation for Example 1: Smart Link ($mJ = 10^{-3} Joule$).	22
1.7	Comparison of two trials of the optimized (Opt) design parameters and resulting energy consumption to perform the morph and percent difference (%Diff) for two angles of deformation with the elliptic path of deformation for Example 1: Smart Link ($\sigma_{tre}^{max} = \ \sigma^{tresca}\ _{L_\infty(\Omega)}$, $mJ = 10^{-3} Joule$).	24

1.8	Control and optimized (Opt) design parameters and resulting energy consumption to perform the morph and percent difference (%Diff) with respect to the control design for two angles of deformation with the elliptic path of deformation with the stress limit reduced to $\sigma^{damage} = 10.0MPa$ for Example 1: Smart Link ($\sigma_{tre}^{max} = \ \sigma^{tresca}\ _{L^\infty(\Omega)}$, $mJ = 10^{-3}Joule$).	25
1.9	Summary of the optimization problem and solution approach for Example 2: Morphing Structural Backbone.	29
1.10	Control and optimized (Opt) design solutions, corresponding resulting temperature distribution at initiation of morphing, and Tresca stress distribution and deformed shape at completion of morphing for the two limit cases on the Pareto surface (minimum energy and minimum curvature deviation) for Example 2: Morphing Structural Backbone ($mJ = 10^{-3}Joule$).	31
2.1	The assumed material parameters for the numerical study.	42
2.2	Applied displacement boundary conditions for Example 1: Smart Link.	48
2.3	Summary of the optimization objective and constraints for Example 1: Smart Link.	49
2.4	Control, optimized design parameters from Genetic Algorithm optimization (GA Opt), optimized design parameters from quasi-Newton gradient-based optimization using the adjoint method (Adjoint Opt), resulting energy consumption to perform the morph, and the percent difference (%Diff) with respect to the control design for Example 1: Smart Link ($mJ = 10^{-3}Joule$).	51
2.5	Applied traction boundary conditions for Example 2: Morphing Structural Backbone.	54
2.6	Summary of the optimization objective and constraints for Example 2: Morphing Structural Backbone.	55
2.7	Optimized (Opt) design solutions (temperature distribution and final stress distribution) with respect to three different target shapes (ellipse, square and step-type) for Example 2: Morphing Structural Backbone.	57
3.1	The assumed material parameters for the numerical study.	66

3.2	Applied traction boundary conditions for Example 1: Morphing Structural Backbone.	72
3.3	Summary of the optimization objective and constraints for Example 1: Morphing Structural Backbone.	73
3.4	Assumed material parameters for linear thermal behavior.	73
3.5	Optimized design solutions (final stress distribution) with respect to three different target shapes (ellipse, square and step-type) for the linear thermal property and the nonlinear thermal property scenarios for Example 1: Morphing Structural Backbone.	75
3.6	Applied traction boundary conditions for Example 2: Morphing Airfoil Structure.	77
3.7	Summary of the optimization objective and constraints for Example 2: Morphing Airfoil Structure.	78
3.8	Optimized design solutions (temperature distribution and final stress distribution) for the linear thermal property and the nonlinear thermal property scenarios for Example 2: Morphing Airfoil Structure.	79

LIST OF FIGURES

1.1	Schematic of the morphing structure design problem in which the applied activation (T^A or q^A) and actuation (\vec{u}^A or $\vec{\tau}^A$) are to be determined to achieve a desired shape change.	5
1.2	Flow chart for the generalized computational design framework.	7
1.3	Assumed relationship between Young’s modulus and temperature for the numerical study.	13
1.4	(a) Schematic of the smart link design concept, (b) two paths of applied displacement considered, elliptic and rectangular, with respect to the angle of deformation, θ , and (c) applied temperature with respect to time for Example 1: Smart Link.	15
1.5	(a) Schematic of the morphing structural backbone design concept and (b) schematic of the parameterization to calculate the curvature deviation design objective for Example 2: Morphing Structural Backbone.	26
1.6	Total energy consumption and final curvature deviation after morphing for the control and Pareto surface of optimal design solutions for Example 2: Morphing Structural Backbone.	30
2.1	The assumed relationship between Young’s modulus and temperature for the numerical study	41
2.2	(a) Schematic of the smart link design concept, (b) the deformation path considered for the top of the structure, and (c) the applied temperature with respect to time for Example 1: Smart Link.	47

2.3	(a) Temperature distribution at initiation of morphing and (b) stress distribution and final deformed shape from optimized design solution from gradient-based optimization using the adjoint method for Example 1: Smart Link. . .	51
2.4	Schematic of the Morphing Structural Backbone Design Concept for Example 2.	53
2.5	Total energy consumption (J) and morphing error (S) for three optimized design solutions with varying weighting parameters (C) for the elliptic target shape for Example 2: Morphing Structural Backbone.	56
3.1	The assumed relationship between Young’s modulus and temperature for the numerical study.	67
3.2	The assumed relationship between thermal conductivity and temperature for the numerical study.	67
3.3	The assumed relationship between specific heat and temperature for the numerical study.	68
3.4	Schematic of Example 1: Morphing Structural Backbone.	71
3.5	Temperature distribution (K) for the morphing system with (a) linear thermal properties and (b) nonlinear thermal properties for Example 1: Morphing Structural Backbone.	74
3.6	Schematic of the Morphing Airfoil Structure Design Concept for Example 2. .	76
3.7	Target Airfoil Shape with 2% Max Camber at Position 40%.	77

PREFACE

First and foremost I wish to thank my advisor Professor John C. Brigham. He has been supportive since the days I began working here. I appreciate all his contributions of time, ideas, and funding to my make my Ph.D. experience productive and simulating. Without his unending faith in my potential and his wonderful and tireless guidance none of my success could have been possible.

I would also like to thank all the committee members of my dissertation, Dr. Jeen-Shang Lin, Dr. Qiang Yu for your academic support and input, especially Dr. Richard Beblo for giving me the suggestion, assistance and guidance to help me complete my dissertation.

I gratefully acknowledge the funding source that made my Ph.D. work possible. I was honored to be a Schlumberger Faculty for the Future Fellow for the last 3 years of my Ph.D. My work was also supported by the U.S. Air Force.

The members of the CDIM group have contributed immensely to my personal and profession at University of Pittsburgh. The group has been a source of friendships as well as good advice and collaboration. I would like to acknowledge the group member Mohammad Ahmadpoor. We worked together on the adjoint problem, and I very much appreciated his enthusiasm, intensity and willingness to help. Other past and present group members that I have had the pleasure to work with or alongside of are Shuai Zhu, Fei Li, Zhanpeng Hao, Jing Xu and Mengyu Wang.

Finally, and most importantly, I would like to thank my family and all their encouragement. For my parents who raised me with love and supported me in all my pursuits. Thank you and love you.

1.0 A COMPUTATIONAL FRAMEWORK FOR THE OPTIMAL DESIGN OF MORPHING PROCESSES IN LOCALLY ACTIVATED SMART MATERIAL STRUCTURES

1.1 ABSTRACT

A proof-of-concept study is presented for a strategy to obtain maximally efficient and accurate morphing structures composed of active materials such as shape memory polymers (SMP) through synchronization of adaptable and localized activation and actuation. The work focuses on structures or structural components entirely composed of thermo-responsive SMP, and particularly utilizes the ability of such materials to display controllable variable stiffness. The study presents and employs a computational inverse mechanics approach that combines a computational representation of the SMP thermo-mechanical behavior with a nonlinear optimization algorithm to determine location, magnitude and sequencing of the activation and actuation to obtain a desired shape change subject to design objectives such as prevention of damage. Two numerical examples are presented in which the synchronization of the activation and actuation and the location of activation excitation were optimized with respect to the combined thermal and mechanical energy for design concepts in morphing skeletal structural components. In all cases the concept of localized activation along with the optimal design strategy were able to produce far more energy efficient morphing structures and more accurately reach the desired shape change in comparison to traditional methods that require complete structural activation prior to actuation.

1.2 INTRODUCTION

There are a variety of engineering application areas with significant ongoing efforts towards smart structure technologies, such as structures or structural components that can actively change their geometry or material behaviors to adapt to and/or alleviate adverse conditions or otherwise improve operational efficiency. For example, the concept of morphing aircraft has been an initiative of the aerospace industry for many years, with objectives of improving a number of flight performance or mission variables. In some sense, morphing aircraft are commonplace if one considers components such as flaps and deployable landing gear. However, in spite of these developments and focused interest, there are a wide variety of components or systems on aircraft that are ideal targets for improved morphing technologies, such as adaptive engine cowlings [73, 74], active clearance control for engine blades [10], and variable geometry chevrons [27, 31].

While many applications of morphing structure technologies have seen solutions of one form or another, the underlying approach has almost always been discretely-actuated mechanisms. Some mechanisms provide the perception of continuous control, in that they deform a smooth surface with an underlying point force, but nonetheless they are still single-degree-of-freedom devices. As such, the achievable shapes/functions are limited to the constraints placed on the original design (i.e. there is no further adaptability beyond the design cases) and practical ability to construct the mechanical degrees of freedom. In addition, most designs involve an actuate-and-hold approach, in which the actuator must hold the device against aerodynamic and/or structural loads when in its “deformed” state, requiring extensive power and actuator strength. Alternatively, a continuously deformable (i.e. intrinsically morphable) structure has conceptually limitless shape-change functionality. Moreover, if the mechanical properties of the structure could also be modified on-demand, shape change could be facilitated through localized softening to minimize required actuation forces or produce multiple shape changes from a single actuation pattern, and then re-hardened to “lock” in the desired shape. This type of structure would provide the freedom of continuous deformability, along with practically applicable actuation forces and the ability to intrinsically support external forces once a desired shape is reached.

Of the structural materials under development for intrinsic morphing technologies, shape memory polymers (SMP) are particularly promising due to their abilities to exhibit controllable variable stiffness through activation and experience extremely large deformations and shape changes without damage and with minimal actuator force requirements. Since their introduction there has been a continual increase in research into the utilization of SMP in a variety of fields and applications [35, 102]. For example, SMP have been used in aerospace applications for deployable structures, morphing aircraft, and deformable wing structures [9, 82, 91], and in medicine for both morphing sutures and stents [5, 63, 75]. There are a wide variety of SMP compositions and properties, and they are divided into three major types based on the stimulus used to bring a change or desired response of the polymer: thermo-responsive [35, 50, 105], chemo-responsive [13, 14, 113], and photo-responsive [4, 8, 29]. There have been efforts to tailor the response of these smart materials, such as through techniques to introduce a gradient transition temperature field [65, 102] or otherwise optimize the distribution to improve the structure’s performance [57, 60, 103]. However, a distinguishing feature of most of the conventional SMP devices existing in the current literature for morphing applications is that the total SMP material is activated through whichever approach was predefined as optimal in order to morph the device [40, 108, 111]. Therefore, the morphing SMP structures are simply replacements for mechanical links, and provide minimal additional functionality (other than their inherent locking and memory ability). By contrast, the current work intends to expand this concept of variable stiffness structural morphing control to the more general case in which arbitrarily localized regions of a structure are softened to enable a desired shape change with minimal effort.

This new approach to morphing structure technology similarly requires a new way of thinking about smart materials and the design or control strategies used to employ them. Instead of a design algorithm determining only forces to achieve desired structural positions, the stimulus (heat in this case) applied to create local changes in the structural material behavior must be included in the design inputs as well. Unfortunately, beyond the simplest possible cases, traditional (i.e. experience-based) design strategies can be expected to be inefficient at best and entirely intractable at worst for these continuously morphable structures. Alternatively, computational design/control strategies that combine numerical

modeling with nonlinear optimization have the potential to address the challenges of this kind of design/control problem. However, the use of these inverse problem solution methods for shape changing structure applications have thus far been limited, and mainly seen in the form of topology optimization and for the design of shape memory alloy (SMA) devices, particularly actuators. Examples include the work in [70], which sought to optimize microactuator geometry, [33] and [100], which sought to design actuator features such as shape and sequencing to control morphing structures, and [47], which aimed to create a generalized design optimization framework for SMA components.

This work presents a proof-of-concept for a new strategy to determine the optimal localized activation and actuation distributions for a morphing SMP structure or structural component to obtain a targeted shape change subject to design objectives such as minimal total required energy. This approach does not require full activation of the SMP, and therefore can uniquely address issues of energy efficiency and efficiency in transition time both in applying and removing activation. For simplicity, the present work focused on thermo-responsive SMP, which is currently the most common class. However, the approach is generalizable to all SMP classes and a wide variety of design objectives and constraints. The general computational inverse problem approach for the continuous SMP design/control problem combines a numerical representation of the morphing process with a nonlinear optimization strategy and is presented in Section 1.3. Then, two example design problems of skeletal structural components are presented in Section 1.4 to show the implementation of the proposed approach as well as the potential benefits and challenges in comparison to a traditional design, followed by the concluding remarks in Section 1.5.

1.3 COMPUTATIONAL DESIGN FRAMEWORK

Figure 1.1 illustrates the general form of the morphing structure design (and analogously control) problems to be considered here. To perform a morphing process for a structure composed of thermo-responsive SMP, some portion of the domain is first heated (or cooled if using a recently developed composition as shown in [21]) with a controllable transient

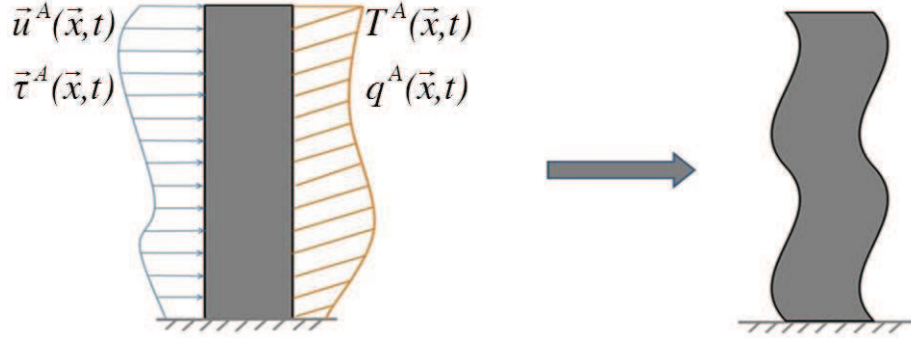


Figure 1.1: Schematic of the morphing structure design problem in which the applied activation (T^A or q^A) and actuation (\vec{u}^A or $\vec{\tau}^A$) are to be determined to achieve a desired shape change.

temperature distribution and/or surface heat flux ($T^A(\vec{x}, t)$ or $q^A(\vec{x}, t)$) (boundary heating is shown and considered in this work, but internally embedded wires have also been used for activation purposes and could be incorporated into this approach). It is critical that the temperature is sufficient to activate the material under the ambient conditions (i.e., bring the internal temperature above the transition temperature), but not so high that the material is damaged. Once a sufficient portion of the structure is softened through activation, mechanical actuation begins through controlled transient displacement and/or force ($\vec{u}^A(\vec{x}, t)$ or $\vec{\tau}^A(\vec{x}, t)$) to deform the structure into the desired final shape. Note that the structure does not necessarily need to be fully activated as in the current standard of practice, but rather only needs to be sufficiently activated to prevent damage, limit the required actuation forces, and ensure that the final shape is maintained once the activation is removed (i.e., the material is cooled and thus rehardened) and actuation is relieved. Furthermore, the process could be synchronized so that the activation proceeds simultaneously with the actuation (i.e., the localized activation does not need to be complete before applying actuation) allowing for the entire process to be particularly efficient.

The design problem to identify the activation and actuation distributions to achieve the desired shape change with maximum efficiency can be cast in a general way in the form of the following constrained multi-objective optimization problem:

$$\text{Minimize : } \begin{cases} \| \vec{u}^{target} - \vec{u}^{approx}(T^A, q^A, \vec{u}^A, \vec{\tau}^A) \|_{\Omega, t_F} \\ J_T(T^A, q^A, \vec{u}^A, \vec{\tau}^A) \\ J_W(T^A, q^A, \vec{u}^A, \vec{\tau}^A) \\ t_F(T^A, q^A, \vec{u}^A, \vec{\tau}^A) \\ g(T^A, q^A, \vec{u}^A, \vec{\tau}^A) \end{cases} \quad (1.1)$$

$$\text{Subject to : } \begin{cases} f(\boldsymbol{\sigma}(\vec{x}, t; T^A, q^A, \vec{u}^A, \vec{\tau}^A)) < \sigma^{damage}, \quad \forall \vec{x} \in \Omega, \quad t \in [0, t_F] \\ T(\vec{x}, t; T^A, q^A, \vec{u}^A, \vec{\tau}^A) < T^{damage}, \quad \forall \vec{x} \in \Omega, \quad t \in [0, t_F] \end{cases} \quad (1.2)$$

where \vec{x} is the spatial position vector, t is the time, Ω is the spatial domain of the structure, t_F is the total time of the morphing process, $\| \cdot \|_{\Omega, t_F}$ is any suitable metric norm with respect to the spatial domain and time, \vec{u}^{target} is the desired displacement (i.e., shape change), \vec{u}^{approx} is the approximate expected displacement given the design parameters predicted by a numerical (or analytical) representation of the structure, J_T and J_W are the total thermal energy and mechanical work, respectively, predicted by the numerical representation to perform the morph, g represents any additional design objectives that may be desired, $\boldsymbol{\sigma}$ and T are the approximate expected internal stress tensor and internal temperature, respectively, predicted by the numerical representation throughout the structure during the morphing process, $f(\cdot)$ is a suitable scalar stress transform (e.g., Tresca criterion), and σ^{damage} and T^{damage} are the stress and temperature limits, respectively, to avoid damaging the material. A solution to 1.1 and 1.2 can be obtained through a nonlinear optimization strategy to identify the activation and actuation parameters that minimize the desired objectives while satisfying the required constraints. Figure 1.2 shows a flow chart that describes the overall procedure for the computational design framework. In general, given the initial structural shape, properties, boundary conditions, and design objectives and constraints, the design problem begins with the generation of one or more trial solutions for the design parameters (i.e., activation and actuation distributions). The suitability of the trials are evaluated using the numerical representation of the structural morphing process, and based on the design criteria

and the optimization strategy employed, the trial solution(s) are updated to better meet the design objectives and the process is repeated. The optimization is completed once a design solution or set of solutions is found that suitably fits the design objectives or a maximum number of iterations is reached.

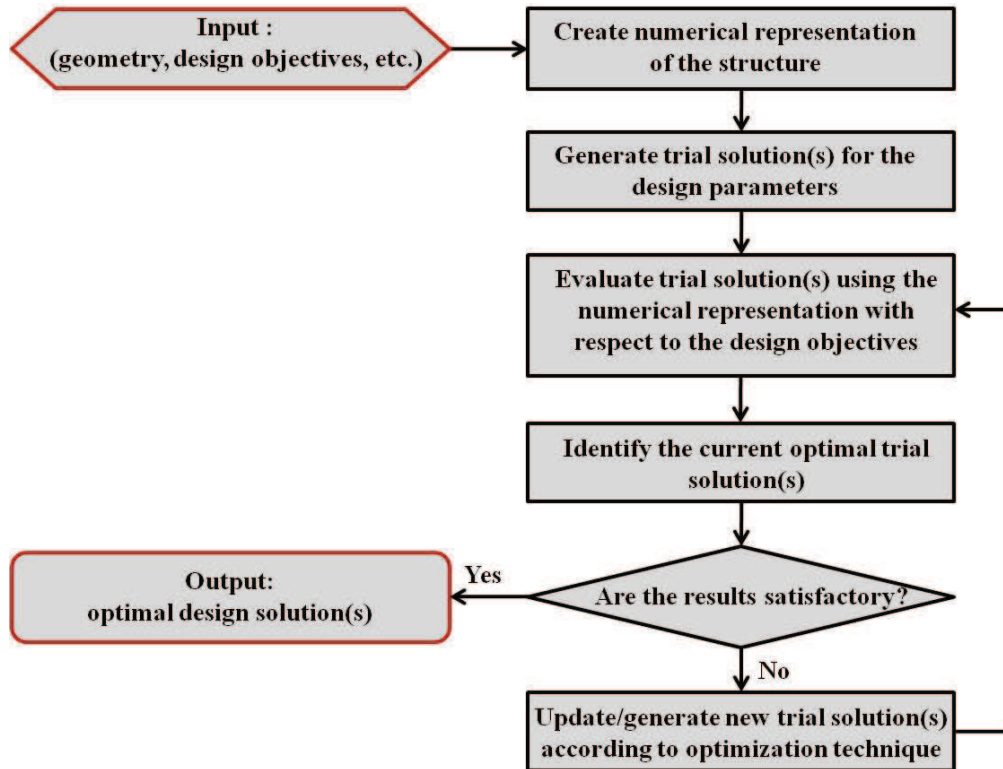


Figure 1.2: Flow chart for the generalized computational design framework.

The computational approach to design a morphing SMP structure used herein primarily relies on the ability to develop a numerical representation (e.g., finite element method, boundary element method, etc.) of the morphing structure that is a reasonably accurate representation of the structural behavior and can predict the morphing outcome (i.e., deformed shape) as well as the outcome of any other design objectives (e.g., total thermal energy input) given an activation and actuation pattern. Any preferred method can be used

to solve the coupled thermo-mechanical SMP analysis to calculate the difference between the desired behavior and the simulated behavior, the total energy (i.e. thermal energy and mechanical work), the total time, and check the constraints for a given set of design parameters. At the continuum level the nonlinear fully coupled thermo-mechanical behavior of thermo-responsive SMP for the vast majority of uses can be theoretically described by the conservation of mass, linear and angular momentum, and energy. Of particular significance to the thermo-responsive SMP case are the conservation of linear momentum and energy, which can be written in general as:

$$\nabla \cdot \boldsymbol{\sigma} + \rho \vec{b} = \rho \vec{\ddot{u}} \quad (1.3)$$

$$\nabla \cdot \vec{q} + \rho e - \rho s = \boldsymbol{\sigma} : (\nabla \vec{\dot{u}}) \quad (1.4)$$

where $\boldsymbol{\sigma}$ is the Cauchy stress tensor, ρ is the mass density, \vec{b} is the body force vector, \vec{u} is the displacement vector, \vec{q} is the internal heat flux vector, e is the internal energy per unit mass, and s is the energy source per unit mass. Of critical importance to computational design problems is that the forward modeling should both accurately and efficiently represent the true physical behavior of the system. Without an accurate representation, an inverse solution may be unattainable, or worse yet, any apparent solution may be dramatically incorrect. Yet, while using multi-physics modeling with the highest possible resolution is ideal from an accuracy standpoint, the resulting computational expense is expected to cause most realistic computational design (particularly control) applications to become infeasible.

Similarly, any preferred optimization approach can be used to guide the search for the optimal design solution. However, the optimization approach should have the capacity to search through wide ranges of parameter values over potentially continuous search spaces and complete the search (i.e., converge) within a reasonable computational expense (i.e. numbers of evaluations of objective functions). In general, optimization techniques can be divided into two major categories: gradient-based and non-gradient based methods. Typically, gradient-based methods can finish the optimization with comparatively few iterations, but are local methods that will seldom find global minima for non-convex problems (which are most common) unless the initial estimate is very close to the global solution. In contrast,

non-gradient based methods, particularly the stochastic search methods such as genetic algorithms, have excellent global search capabilities, but can require a relatively large number of evaluations of the objective functions. In the cases where the systems are particularly complex, each numerical simulation of the system can be of great computational expense, and the number of iterations required for convergence can be prohibitive. In order to successfully obtain solutions for computational design problems it is often desirable to combine the two approaches (i.e. gradient and non-gradient), such as using a stochastic non-gradient method for a relatively small number of iterations first, and then using the obtained estimate as the initial point of a gradient-based local search technique [107], thereby maintaining the global search capabilities with dramatically reduced computational expense.

1.4 NUMERICAL INVESTIGATION OF OPTIMAL DESIGN PROBLEM

As an initial proof-of-concept and to test the inherent benefits and challenges of the proposed computational design approach, a numerical investigation was performed with example design applications derived from concepts of morphing skeletal structural components (i.e., framing and connecting elements). First, a smart link concept was used to extensively explore the potential behavior of the inverse design problem developed herein, including the sensitivity of the design problem to several potential design parameters and the uniqueness of the solution process. Lastly, the example of a morphing structural backbone was considered to explore the ability to account for an indirectly controlled (i.e., not directly actuated) feature of the target shape geometry through localized activation and the computational design approach.

Both example cases followed a standard thermo-responsive SMP cycle for active morphing, in which the structure starts in an initial (cast) configuration, the sample is heated to reduce the stiffness, it is then deformed into a desired new configuration and when the deformation is complete the sample is cooled to restore the stiffness and lock the shape. For simplicity, for all test cases the time required to dissipate the heat and “lock” the structure in the deformed configuration was neglected along with any “bounce back” (i.e., return

deformation) that may occur due to release of residual stress after deforming, removing activation, and releasing actuation forces. However, preliminary tests (not shown for brevity) did indicate that bounce back would likely be negligibly small.

1.4.1 Forward Problem

In all test cases to conserve computing cost the examples were scaled down and simplified considerably so that the activation would occur more quickly and so that the mechanical behavior was reasonably approximated in two dimensions with the plane assumptions. The structures were considered to be composed entirely of SMP and implementation aspects, such as actuation devices and heating elements, were not considered in the analysis beyond their ability to apply temperature ($T^A(\vec{x}, t)$) and displacement ($\vec{u}^A(\vec{x}, t)$) as boundary conditions to the structure. In addition, for simplicity the activation process was assumed to occur entirely through a temperature dependent Young’s modulus, and the behavior of the structures was assumed to be defined by linear transient heat transfer and linear elastic quasi-static solid mechanics. Therefore, the only thermo-mechanical coupling was assumed to be with respect to the Young’s modulus, and the system could be analyzed by a sequentially coupled thermo-mechanical analysis (i.e., an uncoupled thermal analysis sequentially followed by a temperature-dependent mechanical analysis). While these simplifications are noted to be significant and would not be expected to be sufficient for accurately modeling the “true” finite strain nonlinear thermo-mechanical behavior of a thermo-responsive SMP structure being morphed [19, 50, 55, 92], the relative overall behavior and particularly the conclusions drawn with regards to the proof-of-concept of the benefits and challenges of the design methodology should not depend significantly on the simplifications applied herein. Furthermore, initial tests were performed (not shown here for the sake of brevity) comparing the behavior of some of the design solutions for the SMP structures with a simple nonlinear hyperelastic model, as shown in [108], in comparison to the purely linear model. While the nonlinear model showed differences in the stresses occurring during the morphing process, the relative overall stress distributions remained nearly identical and the behaviors predicted using the linear models were generally conservative.

Therefore, the behavior of the SMP devices for the example problems was represented by the following boundary value problem:

$$k\nabla^2 T(\vec{x}, t) = \rho c \frac{\partial T(\vec{x}, t)}{\partial t} \quad \text{in } \Omega, \quad (1.5)$$

$$\nabla \cdot \boldsymbol{\sigma}(\vec{x}, t) = \vec{0} \quad \text{in } \Omega, \quad (1.6)$$

$$\boldsymbol{\sigma}(\vec{x}, t) = \mathbf{C}^{IV}(E(T), \nu) : \boldsymbol{\epsilon}(\vec{x}, t), \quad (1.7)$$

$$\boldsymbol{\epsilon}(\vec{x}, t) = \frac{1}{2}[\nabla \vec{u}(\vec{x}, t) + \nabla \vec{u}(\vec{x}, t)^T], \quad (1.8)$$

$$T(\vec{x}, t) = T^A(\vec{x}, t) \quad \text{on } \Gamma_T, \quad (1.9)$$

$$\vec{u}(\vec{x}, t) = \vec{u}^A(\vec{x}, t) \quad \text{on } \Gamma_U, \quad (1.10)$$

$$k\nabla T(\vec{x}, t) \cdot \vec{n}(\vec{x}) = h(T(\vec{x}, t) - T_{air}) \quad \text{on } \Gamma \cap \Gamma_T, \quad (1.11)$$

where \vec{x} is the spatial position vector, t is the time, T is the temperature, k is the thermal conductivity, ρ is the mass density, c is the specific heat, $\boldsymbol{\sigma}$ is the Cauchy stress tensor, $\boldsymbol{\epsilon}$ is the small strain tensor, \mathbf{C}^{IV} is the fourth order elastic stiffness tensor, E is the Young's modulus, ν is the Poisson's ratio, \vec{u} is the displacement vector, Ω is the spatial domain of the structure, Γ is the domain boundary, \vec{n} is the unit outward normal vector on the domain boundary, Γ_T is the portion of the domain boundary where the temperature is specified, Γ_U is the portion of the boundary where the displacement is specified, h is the convective heat transfer coefficient, and T_{air} is the temperature of the surrounding environment.

Based on the above model, the total thermal energy (J_T) required for activation and the total mechanical work (J_W) required for actuation can then be determined, respectively, with the following:

$$J_T = \int_t \int_{\Gamma_T} -k \nabla T(\vec{x}, t) \cdot \vec{n}(\vec{x}) d\vec{x} dt \quad (1.12)$$

and

$$J_W = \int_t \int_{\Gamma_U} \boldsymbol{\sigma}(\vec{x}, t) \cdot \vec{n}(\vec{x}) \cdot \vec{u}^A(\vec{x}, t) d\vec{x} dt. \quad (1.13)$$

The chosen material parameters were based on those published for the commercially available thermo-responsive SMP Veriflex [15, 44, 53, 62]. Figure 1.3 shows the assumed relationship between the elastic modulus and temperature, with the modulus varying between $1050MPa$ in the glassy (i.e., hard) state to $0.24MPa$ in the rubbery (i.e., soft) state when the SMP is heated above its glass transition temperature, $T_g = 62^\circ C$ or $335.15K$. Furthermore, glass transition rather than melting transition [59, 102] was considered for the present work, and therefore issues relating to latent heat were neglected. The remaining mechanical and thermal material parameters are shown in Table 1.1.

For all analyses (including all test cases and optimization iterations) the coupled thermo-mechanical behavior described by 1.5 - 1.11 was simulated using the Galerkin finite element method [90] through the commercial finite element package Abaqus [96]. Moreover, the finite element analyses were thoroughly verified, particularly with respect to mesh convergence, for the admissible ranges of design parameters considered in all cases.

1.4.2 Optimization Algorithm

The primary tool employed for solving the design optimization problems for the present work was a genetic algorithm, a stochastic global search algorithm that mimics the process of evolution in nature [36, 81]. Genetic algorithms (GAs) are heuristic optimization approaches that generally rely on three main operations to evolve a population of potential solutions to the optimization problem parameters: survival, reproduction, and mutation. In simple terms, survival is the decision process as to which individuals (i.e., potential solutions) progress to the next generation (i.e., stay in the population of potential solutions) based on

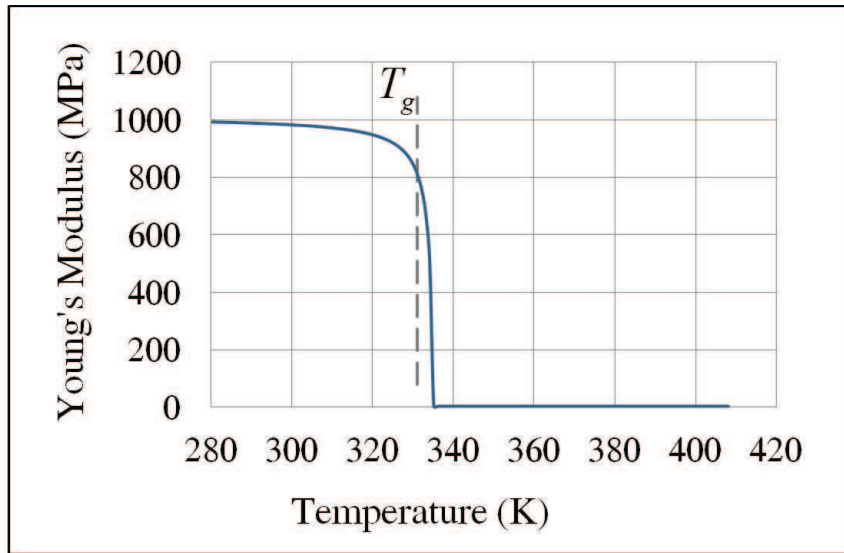


Figure 1.3: Assumed relationship between Young's modulus and temperature for the numerical study.

Table 1.1: Assumed material parameters for the numerical study.

Material Parameter	Value
Poisson's ratio	0.45
Density	$920\text{kg}/(\text{m}^3)$
Specific heat	$1800\text{J}/(\text{kg}\cdot\text{K})$
Thermal conductivity	$0.17\text{W}/(\text{m}\cdot\text{K})$
Convective heat transfer coefficient	$25\text{W}/(\text{m}^2 \cdot \text{K})$

their fitness (i.e., how well the individual meets the optimization objective), reproduction combines parameters for two individuals in the population to create a new individual, and mutation randomly changes a portion of an individual to create a new individual. The evolution of the population continues through several generations until satisfactory individuals are found. GAs have seen substantial use in recent years due to their ease of implementation (e.g., there is no need for complicated gradient calculations), global search capabilities, and simplicity of parallelization. Although GAs may not be ideal for many applications in computational inverse mechanics due to the large number of function evaluations (i.e., numerical simulations) that are typically required to converge to an optimal solution, the relative simplicity of the modeling approach applied herein was certainly a factor in facilitating the use of a GA. Moreover, GAs have seen use in several applications involving SMA or SMP devices [30, 84, 85, 100]. In all example problems presented here, the optimization algorithms were implemented utilizing the toolboxes available within the MATLAB environment [77].

1.4.3 Example 1: Smart Link

The concept of a smart structural link considered here implies a structural element that connects other components of the structural frame (either passive or active structures themselves), which is capable of changing the shape of the structure by changing the positioning of the connected elements through morphing of the link (e.g., [62]). Again note that the design process for such smart link technologies has thus far been largely empirical, usually involving several cycles of fabrication and testing, and the final designs entirely relied on full activation of the SMP component. In contrast, the optimal local activation design approach proposed here seeks to achieve the same target morphing capability more efficiently (i.e., without trial and error testing in the lab) to save time and money in the design process, and create a final design for the activation and actuation process with considerable savings in both time and energy required to morph the structural component.

As shown in Figure 1.4, a $20\text{mm} \times 5\text{mm} \times 1\text{mm}$ homogeneous rectangular prism composed of thermo-responsive SMP was considered and analyzed using the plane stress assumption. Again, note that the size was reduced with respect to in-use structures to reduce computing

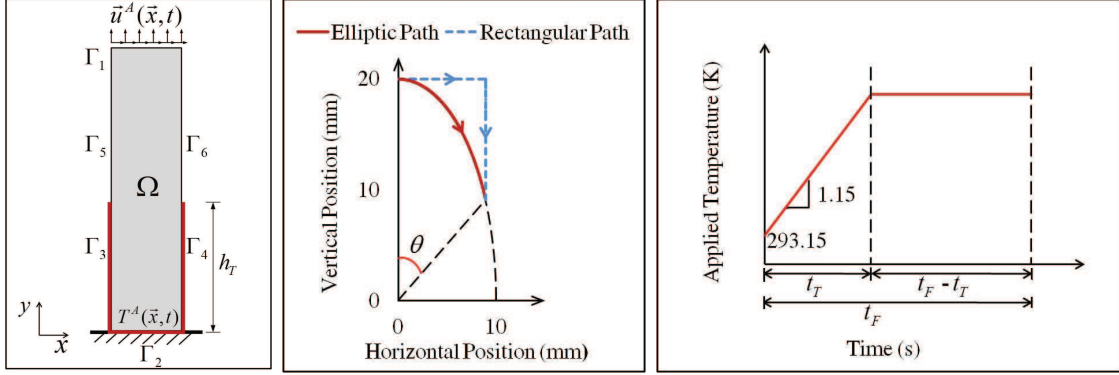


Figure 1.4: (a) Schematic of the smart link design concept, (b) two paths of applied displacement considered, elliptic and rectangular, with respect to the angle of deformation, θ , and (c) applied temperature with respect to time for Example 1: Smart Link.

costs, but the observations with respect to the inverse procedure should not be significantly affected by the size of the structure. The morphing procedure considered involved first heating the structure in its cast configuration to initiate the activation process. After some time of purely heating actuation would be applied to deform the structure into the desired shape. As such, the total time to perform the structural morph, t_F , was simply the summation of the purely heating time, t_D , and the actuation time, t_M .

For the mechanical actuation process the bottom of the structure (Γ_2) was assumed to be fixed to a rigid support and the displacement across the top of the structure (Γ_1) was uniformly controlled to meet the target deformation (i.e., actuation was applied only to the top surface, and the target shape change only applied to the top surface). For comparison purposes, two different deformation paths were considered to reach the same targeted final shape based on the change in angle along the path of an ellipse as shown in Figure 1.4: (1) a path that followed the curve of the ellipse (referred to as the elliptic path) and (2) a purely horizontal motion followed by a purely vertical motion (referred to as the rectangular path). In addition, actuation was assumed to occur at a constant rate. Therefore, the actuation process could be defined completely by the path type (elliptic or rectangular), the final angle of deformation, θ , the starting time, t_D , and the time to complete the deformation (i.e.,

Table 1.2: Applied displacement boundary conditions for Example 1: Smart Link.

Mechanical boundary Type	$0 \leq t \leq t_D$	$t_D \leq t \leq t_F$
	$u_1(t) = 0$	$u_1(t) = 0$
Fixed boundary (Γ_2)	$u_2(t) = 0$	$u_2(t) = 0$
	$u_1(t) = 0$	$u_1(t) = \sqrt{\frac{400 \tan^2(\theta(t-t_D)/t_M)}{4 \tan^2(\theta(t-t_D)/t_M)+1}}$
Elliptic path (Γ_1)	$u_2(t) = 0$	$u_2(t) = 20 - \sqrt{\frac{400}{4 \tan^2(\theta(t-t_D)/t_M)+1}}$
	$u_1(t) = 0$	$u_1(t) = \frac{20(\sqrt{4 \tan^2 \theta + 1} + \tan \theta - 1)(t-t_D)}{(\sqrt{4 \tan^2 \theta + 1})t_M}$
Rectangular path (Γ_1)	$u_2(t) = 0$	$u_2(t) = \frac{20(\sqrt{4 \tan^2 \theta + 1} + \tan \theta - 1)(t-t_D) - 20 \tan \theta \cdot t_M}{(\sqrt{4 \tan^2 \theta + 1})t_M}$

morph), t_M , as shown in terms of the displacement boundary conditions in Table 1.2. The remaining boundaries (Γ_3 , Γ_4 , Γ_5 , and Γ_6) were taken to be traction free.

For the thermal activation process the entire structure was assumed to be initially at room temperature ($293K$) and temperature was assumed to be controllable with a heating element along the entire bottom (i.e., the support region) and along some portion of both sides starting from the bottom (i.e., the height of the heating element, h_T , was assumed to be controllable). Temperature was assumed to be applied uniformly to the heating region (Γ_2 , Γ_3 , and Γ_4) and to increase linearly on that region starting from room temperature at a fixed rate of $1.15K/s$ for a controllable “warm-up” duration (in effect defining the maximum applied temperature), t_T , and then held constant until morphing was completed, as shown in Figure 1.4. The portion of the boundary not being heated (Γ_1 , Γ_5 , and Γ_6) was assumed to be exposed to air at room temperature ($T_{air} = 293K$) with a convective boundary condition and convective heat transfer coefficient (h) of $25W/(m^2 \cdot K)$.

The primary design objective of this first example was to minimize the total (thermal and mechanical) energy to obtain the specified shape change without damaging the structure. Based on the example concept for a smart link structure, the potential variables for optimizing the design of the thermal activation and mechanical actuation included: warm-up time (i.e., time to increase applied temperature) (t_T), heating time prior to actuation (t_D), height

of the heating element (h_T), and actuation time (t_M). As a point of comparison throughout the example a “control” design was established based on the traditional implementation resembling the current standard of practice for a thermo-responsive SMP morphing structure concept. For the control design the heating element was applied to the maximum boundary area and the applied temperature was raised to the maximum level. Only after the entire volume of the structure was activated (i.e., the entire domain temperature reached a value greater than T_g) the actuation was applied to deform the structure as quickly as possible. Note that the variables required to fully activate the structure prior to actuating are independent of the actuation path or total deformation and the minimal morphing time was assumed to be constant, therefore, the control design parameters remained constant for all test cases. The parameters used for the control design were given by

$$t_T = 100s, t_D = 100s, h_T = 20mm, t_M = 10s. \quad (1.14)$$

One last important step prior to setting up the optimization problem was to test and evaluate the effect of the design variables on the design objectives (i.e., the sensitivity of the design variables). In general, towards reducing the ill-posedness of the inverse design problem, the optimization process should include only those variables that have a significant effect on the design objectives.

1.4.3.1 Sensitivity Analysis: To test the relative effect of the four potential design variables on the design objectives a coarse sensitivity analysis was performed in which the parameters used for the control analysis were modified one at a time (with the other three variables held constant at the original control design values). The morphing process was simulated for the elliptic path with an angle of deformation of $\pi/4 rad$ for each variation to determine the relative change in the total activation and actuation energy. Each variable was modified by two amounts, 20% and 40%, in turn, and Table 1.3 shows the relative change in the total energy compared to the control design with respect to each design variable. Note that the sensitivity results for the given path and angle of deformation were representative of the behavior of the alternate path and other angles of deformation (further tests are not shown for brevity). The results presented are fairly simple, but important, showing a high

Table 1.3: Relative (percent) change in total energy to complete the morph for changes of 20% and 40% for each potential design variable, respectively, for the elliptic path and angle of deformation $\theta = \pi/4 rad$ for Example 1: Smart Link.

Design Parameters	Total energy change% (20% Parameter change)	Total energy change% (40% Parameter change)
t_T	14.1	32.6
t_D	9.6	14.9
h_T	13.5	32.4
t_M	1.3	2.4

dependence for the total energy on the warm-up time, t_T , and the height of the heating element, h_T , slightly less dependence on the heating time prior to actuation, t_D , and a minimal dependence on the actuation time, t_M . One additional interpretation of the sensitivity results is that the thermal energy dominates the efficiency of the thermo-responsive SMP device in comparison to the mechanical actuation, which confirms an expected outcome when considering the current literature and emphasis on applying and relieving activation efficiently. As such, including the actuation time would only serve to “confuse” the search process (i.e., increase the ill-posedness of the problem) by having nearly identical outcomes for very different parameter values and would provide minimal potential benefit to the design objective. Therefore, the actuation time was eliminated from the optimization process and simply fixed at a value of $t_M = 10s$, and the design optimization included the remaining three design variables:

- Warm-up time (t_T).
- Heating time prior to actuation (t_D).
- Height of the heating element (h_T).

Table 1.4: Summary of the optimization problem and solution approach for Example 1: Smart Link.

Objective Function	$f = J_T + J_W + J_{max} \cdot \frac{\ \sigma^{tresca}\ _{L_\infty(\Omega)}}{\sigma^{damage}} \cdot H(\ \sigma^{tresca}\ _{L_\infty(\Omega)} - \sigma^{damage})$
Design Parameters	$0 < t_T \leq 100s$
and Constraints	$0 < t_D \leq 590s$ $0 < h_T \leq 20mm$
Optimization Method	Hybrid Genetic Algorithm – Interior Point Method

1.4.3.2 Optimization Problem: Once the sensitive design parameters were established, the optimization approach was implemented to optimally design the thermo-responsive SMP smart link to minimize the total activation and actuation energy to achieve the shape change without damaging the structure. Table 1.4 shows an outline of the constrained optimization problem constructed and the solution approach. For this first example the design objective was cast as a single objective to minimize the total combined energy (i.e., the sum of the thermal energy and mechanical work). The constraints included the maximum total time to complete the morph of 600s, the maximum height of the heating element of 20mm (i.e., the total height of the device), the maximum temperature to prevent damage of 408K, which was implemented by constraining the warm-up time (t_T) to a maximum of 100s, and the maximum Tresca stress ($\|\sigma^{tresca}\|_{L_\infty(\Omega)}$) to prevent damage of 11.5MPa. An additional note is that the stress constraint was particularly challenging to implement as it was the one constraint that did not directly relate to a design parameter. During development the stress constraint was initially implemented as a “hard” constraint by severely and equally penalizing all individuals that exceeded the stress limit anywhere in the domain. However, the “hard” constraint caused the search process to be far more challenging than expected since there was no guidance for the search to lead toward a possible optimum near to the stress limit. To overcome this difficulty, the maximum stress constraint was incorporated as

an additive penalty function in the objective function to improve the design optimization search space. The penalty function was formulated as a ramp function as follows

$$J_{max} \cdot \frac{\|\sigma^{tresca}\|_{L_\infty(\Omega)}}{\sigma^{damage}} \cdot H(\|\sigma^{tresca}\|_{L_\infty(\Omega)} - \sigma^{damage}) \quad (1.15)$$

where $H(\cdot)$ is the Heaviside step function, $\|\cdot\|_{L_\infty(\Omega)}$ is the L_∞ -norm over the domain Ω , and J_{max} is the estimated maximum possible value of total energy. This ramp function penalty prevented solutions that violated the constraint without penalizing or even differentiating those below the limit condition. However, the penalty function allowed the optimization procedure to differentiate between solutions that were close to admissible versus those which were not, thereby dramatically improving the simplicity of the design solution search space.

Initial testing (not shown here for brevity) showed that the energy functions (1.12 and 1.13) were substantially non-convex, and therefore, the selected optimization approach of a GA was well-suited for the problems herein. Three common operators were used for the GA in this example: stochastic uniform sampling as the selection operator, single point crossover as the reproduction operator, and the adaptive feasible mutation operator. In addition, to ensure that the optimization solutions were locally refined as much as possible for the first example, the design solution provided by the GA was implemented as the initial guess in a gradient based optimization algorithm known as the interior point optimization method [37, 38, 68]. Specifically, the Hessian was calculated by a dense quasi-Newton approximation in which both Newton steps and conjugate gradient steps were allowed at each iteration (i.e. the algorithm first attempts to take a Newton step and if the algorithm cannot, a conjugate gradient step is taken.), and the functions were scaled by their values at the initial point. However, in general the gradient-based optimization provided minimal improvement to the solution beyond what was provided by the GA.

1.4.3.3 Optimization Results and Discussion: Table 1.5 shows both the control and optimized design parameter values for the warm-up time (t_T), heating time (t_D), and height of heating element (h_T), and the corresponding activation thermal energy (J_T), actuation mechanical work (J_W), and total energy (J), and the percent difference with respect to the control designs for the elliptic path with two angles of deformation, $\pi/10 rad$ and $\pi/4 rad$.

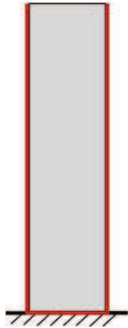
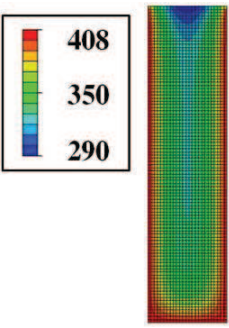
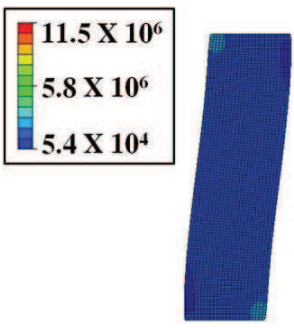
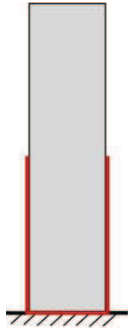
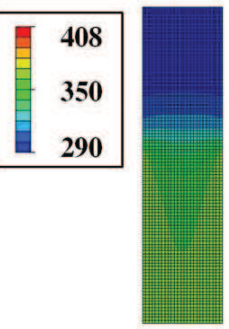
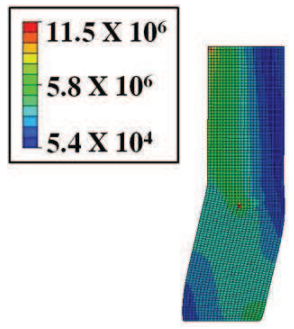
Table 1.5: Control and optimized (Opt) design parameters and resulting energy consumption to perform the morph and percent difference (%Diff) with respect to the control design for two angles of deformation with the elliptic path of deformation for Example 1: Smart Link ($\sigma_{tre}^{max} = \|\sigma^{tresca}\|_{L^\infty(\Omega)}$, $mJ = 10^{-3} Joule$).

θ (rad)	Design Case	t_D (s)	t_T (s)	h_T (mm)	σ_{tre}^{max} (MPa)	J_T (mJ)	J_W (mJ)	J (mJ)
$\pi/10$	Control	100.0	100.0	20.0	1.3	16915.0	4.0	16919.0
	Opt	74.6	84.3	8.1	11.5	5900.3	18.2	5918.5
	%Diff	-25.4	-15.7	-59.7	+812.9	-65.1	+357.3	-65.0
$\pi/4$	Control	100.0	100.0	20.0	3.3	16915.0	42.1	16957.1
	Opt	101.5	66.6	10.8	11.5	7819.0	88.9	7907.9
	%Diff	+1.5	-33.4	-46.2	+250.3	-53.8	+111.1	-53.4

In addition, Table 1.6 shows a representative example of the temperature at initiation of morphing and the Tresca stress distributions and the final deformed shape of the optimized design compared to the control design for the elliptic path with the angle of deformation $\pi/4 rad$.

In all cases a substantial energy savings was obtained from the optimal design process, with a reduction in total energy consumption of over 50% regardless of the angle of deformation in comparison to the control design. Yet, while the total energy was lower, the mechanical work portion of the energy was much higher for all of the optimized designs compared to the control design, with an increase of over 100% for the larger deformation and over 300% for the smaller deformation. Furthermore, all optimal design solutions had a maximum Tresca stress during the morphing process very near to the stress limit (i.e., damage stress) (shown after rounding up as the exact value). In particular, the mechanical portion of the results further emphasizes what was noted previously that the thermal energy

Table 1.6: Control and optimized (Opt) design solutions, resulting temperature distribution at initiation of morphing, and Tresca stress distribution and deformed shape at completion of morphing for angle of deformation $\pi/4 rad$ with the elliptic path of deformation for Example 1: Smart Link ($mJ = 10^{-3} Joule$).

Design Case	Schematic	Temperature Distribution (K)	Stress Distribution (Pa)
Control $t_D = 100.0s$ $t_T = 100.0s$ $h_T = 20.0mm$ $J = 16957.1mJ$			
Opt $t_D = 101.5s$ $t_T = 66.6s$ $h_T = 10.8mm$ $J = 7907.9mJ$			

dominated the energy consumption of the morphing process. Therefore, not surprisingly the primary objective of the optimization naturally became identifying the applied heating to minimally activate the structure to prevent damage during the morph.

As would be expected, the optimized design solutions and resulting improvements in the energy consumption are noticeably different depending on the angle of deformation and there is a nonlinear relationship between the optimized solution and the final morphed shape. However, the optimized design solutions and resulting improvements in the energy consumption are nearly identical for different actuation paths (elliptic or rectangular), hence only one set of results are presented. The path results can in part be explained by the relative path independence as well as the relative insignificance of the mechanical work to the total energy requirement. Moreover, testing showed that in many instances different design parameter combinations resulted in nearly identical total energy solutions, which further highlights the ill-posedness that creates a challenge for the inverse problem.

To explore the relative uniqueness of the potential design solutions and in some sense the ill-posedness of the inverse problem in a simple way, several additional optimization tests were performed to identify alternate solutions near to the optimal total energy requirement, but with varying design parameters. Table 1.7 shows examples of design solutions with similar total energy consumption as the previous optimized solutions for the elliptic actuation path, but with disproportionately different design parameter values. Of note is that in the elliptic path with $\theta = \pi/10 \text{ rad}$ the thermal energy was higher while the mechanical work was lower in comparison to the original optimal solution, which may be a critical difference depending on the specifics of the application such as a preference for lower mechanical energy consumption regardless of increases to thermal cost. Fortunately, the computational design strategy is such that emphasis could easily be placed on either cost functional component (mechanical or thermal) with weighting functions if the user had priority on minimizing the mechanical work more so than thermal or vice versa. Furthermore, to create a comprehensive view of the design options one could systematically vary the weighting on the cost functional components or employ some other variant of a multi-objective optimization approach to obtain the spectrum of potential design solutions (i.e., Pareto surface) with respect to energy (or any other design target) tradeoffs. Overall though, these results clearly show the impact

Table 1.7: Comparison of two trials of the optimized (Opt) design parameters and resulting energy consumption to perform the morph and percent difference (%Diff) for two angles of deformation with the elliptic path of deformation for Example 1: Smart Link ($\sigma_{tre}^{max} = \|\sigma^{tresca}\|_{L_\infty(\Omega)}$, $mJ = 10^{-3} Joule$).

θ (rad)	Deisgn Case	t_D (s)	t_T (s)	h_T (mm)	σ_{tre}^{max} (MPa)	J_T (mJ)	J_W (mJ)	J (mJ)
$\pi/10$	Opt1	74.6	84.3	8.1	11.5	5900.3	18.2	5918.5
	Opt2	92.0	61.0	8.8	11.5	5906.1	16.6	5922.7
	%Diff	+23.2	-27.6	+9.0	0.0	+0.1	-8.8	+0.1
$\pi/4$	Opt1	101.5	66.6	10.8	11.5	7819.0	88.9	7907.9
	Opt2	118.3	64.4	10.6	11.5	7877.3	89.7	7967.0
	%Diff	+16.5	-3.3	-1.2	+0.0	+0.7	+0.9	+0.7

of the computational design approach to significantly improve the efficiency of potential morphing devices.

Lastly, based on the premise that in practice a design solution that produces internal stresses near to damaging the structure (which was the case for all optimized solutions) would be undesirable, an additional set of tests were performed in which the stress limit was reduced and the optimization repeated. Table 1.8 shows the results of the design optimization process with the maximum Tresca stress set to a value of 10 *MPa* instead of the 11.5 *MPa* used previously. Similarly to the previous results all of the optimal design solutions had a maximum Tresca stress during the morphing process very near (exact after rounding) to the new stress limit. The results imply that at least for the present example the optimal design will generally yield a stress near to the maximum stress constraint, which again is largely based on the dominance of the thermal energy in the overall efficiency of the device. Moreover, the solution design parameters were again quite different than the previous test cases further emphasizing the diversity of the potential design solutions.

Table 1.8: Control and optimized (Opt) design parameters and resulting energy consumption to perform the morph and percent difference (%Diff) with respect to the control design for two angles of deformation with the elliptic path of deformation with the stress limit reduced to $\sigma^{damage} = 10.0MPa$ for Example 1: Smart Link ($\sigma_{tre}^{max} = \|\sigma^{tresca}\|_{L^\infty(\Omega)}$, $mJ = 10^{-3}Joule$).

θ (rads)	Design Case	t_D (s)	t_T (s)	h_T (mm)	σ_{tre}^{max} (MPa)	J_T (mJ)	J_W (mJ)	J (mJ)
$\pi/10$	Control	100.0	100.0	20.0	1.3	16915.0	4.0	16919.0
	Opt	95.8	63.3	8.7	10.0	6089.7	14.5	6104.2
	%Diff	-4.2	-36.7	-56.6	+693.9	-64.0	+264.4	-63.9
$\pi/4$	Control	100.0	100.0	20.0	3.3	16915.0	42.1	16957.1
	Opt	142.6	59.1	12.3	10.0	8611.8	80.4	8692.2
	%Diff	+42.6	-40.9	-38.6	+204.6	-49.1	+91.0	-48.7

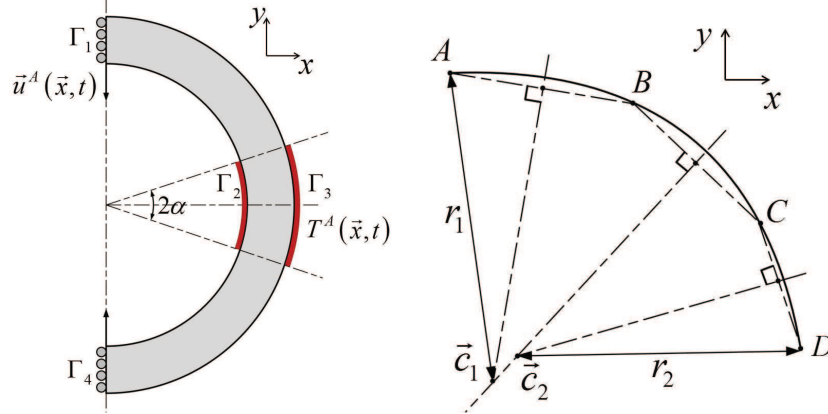


Figure 1.5: (a) Schematic of the morphing structural backbone design concept and (b) schematic of the parameterization to calculate the curvature deviation design objective for Example 2: Morphing Structural Backbone.

1.4.4 Example 2: Morphing Structural Backbone

In contrast to the smart link, the concept of the morphing structural backbone considered here implies a structural element that is more directly connected to the exposed surface of the structure, and therefore, the overall shape of the backbone, not just the positioning of endpoints, affects the functional shape of the structure. For example, such a morphing component could be installed in the edge of an aerodynamic structure such as a wing, in which it may be desirable to use the component to prescribe both the size as well as the shape (e.g., curvature) of the edge surface. The structural backbone considered for the second example is shown in Figure 1.5. The structure was taken to be a homogeneous half-circular prism with $20mm$ outer radius, $15mm$ inner radius, and $200mm$ length composed of thermo-responsive SMP, and the structure was analyzed using the plane strain assumption.

The morphing procedure applied followed a nearly identical sequencing pattern as the first example, with the exception that the warm-up duration (t_T) was eliminated and the applied temperature was assumed to be instantaneously fixed at the start of activation as the maximum value of $408K$. Similarly to the previous example, the time to complete the

deformation (t_M) did not have a significant effect on the design objectives and was again fixed at a value of 10s. For the mechanical actuation process the two ends of the structure (Γ_1 and Γ_4) were assumed to be constrained in the horizontal direction and the vertical displacement was uniformly controlled to deform each end toward the centerline of the structure (effectively reducing the height of the structures profile). For the thermal activation process the entire structure was assumed to be initially at room temperature (293K) and a portion of the outer and inner surface of the structure defined by the angle α (Γ_2 and Γ_3) was heated with the fixed temperature of 408K. The remaining (unheated) boundaries of the structure were assumed to be insulated. Therefore, the variables to optimize the design of the morphing backbone included:

- Heating time prior to actuation (t_D).
- Angle of the heating element (α).

Due to the symmetry of the structure, all analyses were performed considering only the top half of the morphing backbone.

Two design objectives were considered for this second example in addition to the constraint to prevent damage: (1) minimize the total energy required to perform the morphing process (identically to the first example through the sum of 1.12 and 1.13) and (2) maintain a curvature over the outer surface as close to circular as possible (i.e., to maintain the half circle shape). Figure 1.5 shows a schematic for the approach used to parameterize the curvature objective. For simplicity, the curvature objective calculation divided the outer surface of the structure into three equal sections: \overline{AB} , \overline{BC} and \overline{CD} . Then the relative difference between the achieved curvature after morphing and that of a circle (referred to as the “curvature deviation” (d)) was defined as the relative difference between the intersection points of the perpendicular bisectors of \overline{AB} and \overline{BC} (\vec{c}_1) compared to \overline{BC} and \overline{CD} (\vec{c}_2) with respect to the average of the corresponding radii of curvature for \overline{ABC} (r_1) and \overline{BCD} (r_2), given by:

$$d = \frac{\sqrt{(c_{1x} - c_{2x})^2 + (c_{1y} - c_{2y})^2}}{0.5(r_1 + r_2)}. \quad (1.16)$$

Again, for a point of comparison throughout the second example a control design was established based on complete activation of the structure prior to actuation. For the control design, the entire outer and inner surfaces of the structure were heated and actuation was applied after the entire volume was activated, yielding the following control design parameters:

$$t_D = 25s, \alpha = \pi/2 \text{ rad.} \quad (1.17)$$

1.4.4.1 Optimization Problem: Table 1.9 shows an outline of the constrained multi-objective optimization problem for the morphing backbone. Again, a GA was employed to solve the optimization problem, but in this case with a multi-objective approach to address the two competing objectives and without the additional gradient based algorithm at completion. The multi-objective GA applied used a Pareto-based ranking scheme with the tournament selection operator, single point crossover, and adaptive feasible mutation to identify a set of design solutions along the Pareto front representing the spectrum of optimal combinations of total energy and curvature deviation. An important note is that for this example it was necessary to implement the ramp function stress penalty on both optimization objectives (energy and curvature), otherwise solutions that violated the stress limit would be admissible on the Pareto surface. For the curvature deviation penalty d_{max} is the estimated maximum possible value of curvature deviation.

1.4.4.2 Optimization Results: Figure 1.6 shows the Pareto surface of the optimal solutions obtained for the morphing backbone. As can be seen, every optimized solution had improvement in both objectives, using less total energy and achieving a smaller curvature deviation in comparison to the control design case. In addition, the Pareto surface shows a nearly linear tradeoff relationship between the total energy and the curvature. Table 1.10 shows the optimized design solutions, the corresponding temperature distributions at the initiation of morphing, the final Tresca stress distributions, and the final deformed shapes for the two limit points on the Pareto surface (i.e., absolute minimum energy and minimum curvature deviation) compared to the control design. Similar to the first example, consider-

Table 1.9: Summary of the optimization problem and solution approach for Example 2: Morphing Structural Backbone.

Objective Functions	$f_1 = J_T + J_W + J_{max} \cdot \frac{\ \sigma^{tresca}\ _{L_\infty(\Omega)}}{\sigma^{damage}} \cdot H(\ \sigma^{tresca}\ _{L_\infty(\Omega)} - \sigma^{damage})$ $f_2 = d + d_{max} \cdot \frac{\ \sigma^{tresca}\ _{L_\infty(\Omega)}}{\sigma^{damage}} \cdot H(\ \sigma^{tresca}\ _{L_\infty(\Omega)} - \sigma^{damage})$
Design Parameters	$0 < t_D \leq 590s$
and Constraints	$0 < \alpha \leq \pi/2 rad$
Optimization Method	Multi-objective Genetic Algorithm

ably less heat was applied in the optimized solutions compared to the control design, and a locally activated solution was optimal in all cases. It is of particular interest that regardless of the energy consumption, local activation is necessary to accurately achieve the desired shape change, and the computational approach is particularly well suited to determine this activation in contrast to intuitive design approaches. Again, the only drawback of the local activation might be the relatively high stress distributions that occur during morphing in comparison to the control design. Although, in all cases the stress occurring for the optimized cases was within the reasonable range assumed to not cause damage.

1.5 CONCLUSION

A strategy for utilizing synchronized and localized activation and actuation for optimally efficient morphing smart material structures was presented and analyzed. For context the presentation focused on thermo-responsive shape memory polymer structures and structural components, and a computational inverse mechanics methodology was proposed for determining the parameters defining the necessary applied thermal activation and mechanical actuation to optimally design morphing processes for such structures. The inverse solution

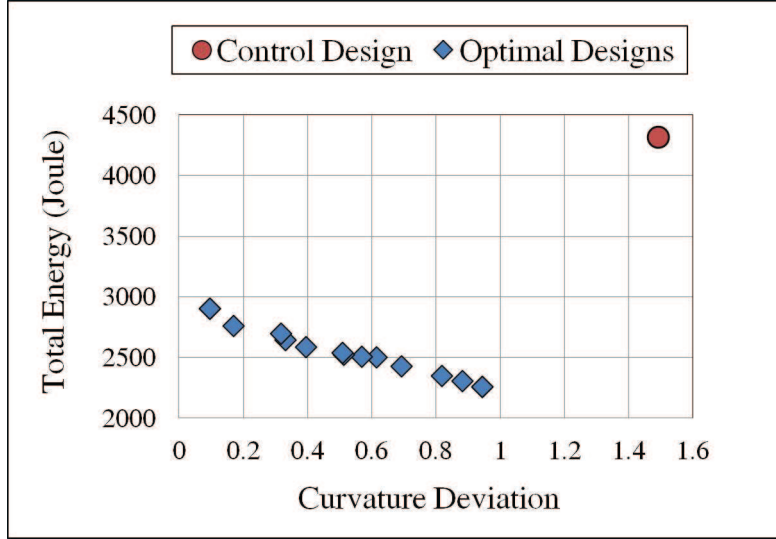
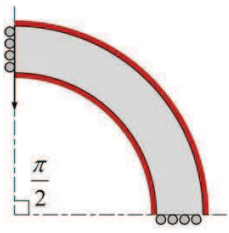
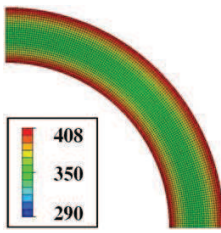
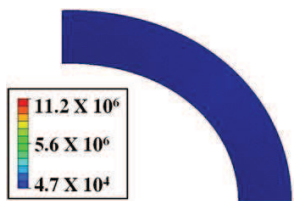
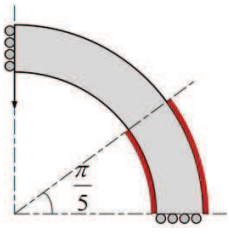
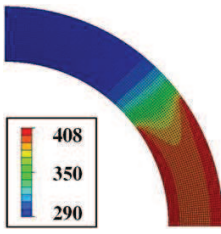
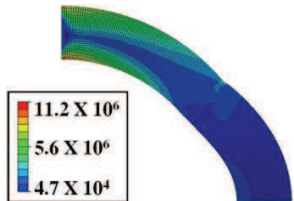
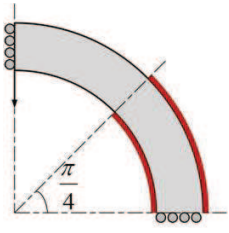
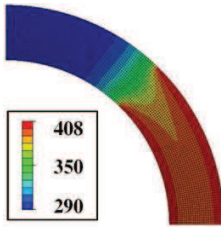
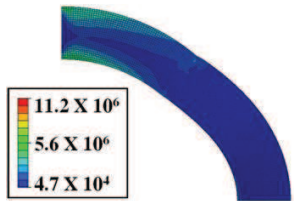


Figure 1.6: Total energy consumption and final curvature deviation after morphing for the control and Pareto surface of optimal design solutions for Example 2: Morphing Structural Backbone.

approach included a computational representation of the coupled thermo-mechanical behavior during the morphing process and a nonlinear optimization algorithm to identify the design parameters that yield a morphing process that best approximates the desired shape change subject to design objectives such as minimal morphing time, energy costs, and damage prevention. Then a numerical study was shown consisting of two example design concepts based on simplified morphing skeletal structural components with temperature-dependent elastic moduli (representing thermo-responsive SMP) as a proof of concept to analyze the effectiveness of the smart structure concept and design strategy. The finite element method was employed to simulate the thermo-mechanical morphing processes and a genetic algorithm combined (when possible) with an interior point method was used to identify the applied thermal activation and mechanical actuation to optimally approximate the desired shape change and minimize the total combined applied thermal and mechanical energy without damaging the material. Through the numerical study, the framework was shown to provide a generalized and flexible means to dramatically improve efficiency of a shape-changing

Table 1.10: Control and optimized (Opt) design solutions, corresponding resulting temperature distribution at initiation of morphing, and Tresca stress distribution and deformed shape at completion of morphing for the two limit cases on the Pareto surface (minimum energy and minimum curvature deviation) for Example 2: Morphing Structural Backbone ($mJ = 10^{-3} \text{ Joule}$).

Design Case	Schematic	Temperature Distribution(K)	Stress Distribution(Pa)
Control $t_D = 25s$ $\alpha = \pi/2$ $J = 4321.2mJ$ $d = 1.5$			
Opt1 $t_D = 49.4s$ $\alpha = \pi/5$ $J = 2257.0mJ$ $d = 0.9$			
Opt2 $t_D = 57.6s$ $\alpha = \pi/4$ $J = 2903.6mJ$ $d = 0.1$			

structure over more traditional (and intuitive) approaches that require full activation of the structure prior to actuation. However, some challenges were also identified for the solution strategy including substantial non-convexity of the optimization search spaces and solution non-uniqueness, which significantly hinder the efficiency of the solution process and without further developments may limit the practical applicability of these strategies to more elaborate structures and more realistic representations of the smart material behavior that demand far more computing power.

2.0 A COMPUTATIONALLY EFFICIENT APPROACH FOR OPTIMAL DESIGN OF SMART MATERIAL MORPHING STRUCTURES USING THE ADJOINT METHOD

2.1 ABSTRACT

A computational strategy is presented for computationally efficient estimation of the optimal parameters relating to the distribution and sequencing of activation and actuation for a morphing smart material structure or structural component to efficiently and effectively achieve a desired morphing function. The strategy was presented in the context of structures or structural components composed entirely of thermally responsive shape memory polymer, and combines a numerical representation of the morphing process with a nonlinear optimization algorithm to estimate the activation and actuation parameters that best address cost functions and constraints relating to energy consumption, target shape change(s), morphing time, and/or damage prevention. In particular, a formulation of the adjoint method is presented to be utilized to estimate the gradient of the objective function(s) with respect to the activation and actuation parameters with minimal computational expense within a gradient-based optimization strategy, which then provides an optimization process that is substantially computationally efficient overall. Two numerical examples are presented to verify and test the computational approach, in which the synchronization of multiple activation and actuation parameters was optimized with respect to the energy cost and target shape changes in morphing skeletal structural components. Overall, the computational optimal design approach with the adjoint method was shown to provide the capability to efficiently identify activation and actuation parameters to achieve desired morphing capabilities.

2.2 INTRODUCTION

Morphing structure technologies have a myriad of potential applications in the realm of reconfigurable and/or adaptable structures. Examples of such technologies include: transformable structures, which may conform to uncertain and emergent situations by changing according to occupant demand or energetic considerations [18, 41, 83]; deployable structures, which may change configurations depending on the service requirement [2, 46, 104]; and morphing aircraft, which may allow an aircraft to adapt in flight to meet changing mission objectives or environments [7, 23, 54]. There is a broad range of research efforts seeking solutions for the implementation of these morphing structure concepts described, including efforts relating to mechanisms to facilitate morphing as well as the manufacturing processes to build such structures. Concomitantly, a large amount of current research focuses on the integration of new materials into morphing structure concepts. Of particular interest have been smart active materials that have intrinsically controllable material properties. Such materials could conceptually provide for infinite possibilities in the types of structures that could be created and the morphing capabilities they could employ.

Among the smart materials being developed, Shape Memory Polymers (SMPs) are a particularly promising class of structural materials that have the ability to exhibit variable stiffness and experience extremely large deformations and shape changes without damage and with minimal actuator force requirements. There are a wide variety of SMP compositions and properties, and they can typically be divided based on the stimulus used to bring about a change or desired response of the polymer. The most common is the thermally responsive SMP [26, 118], followed by electrically responsive [109, 112], light responsive [39, 58], and chemically responsive [11, 12]. SMPs have already seen utilization in some of the aforementioned morphing technologies, including deployable structures [42, 116], morphing aircraft [69, 115, 117], as well as in medicine, for both morphing sutures and stents [64, 110], among other applications [66, 67].

The design space for morphing structures composed of smart materials is truly open-ended. Unfortunately, beyond the simplest possible cases, traditional (i.e., experience-based) design strategies can be expected to be inefficient and likely ineffective, and alternative tools

for implementing these technologies have not yet been extensively explored. A potential strategy to overcome these design challenges is to use a computational inverse mechanics approach. For a typical computational inverse mechanics approach, a numerical representation (e.g., finite element model) of the smart material system under consideration is first created. An objective function and corresponding set of constraints are then defined that measure the difference between the numerically approximated response given a set of unknown variables and the system behavior that is desired. Lastly, a nonlinear optimization algorithm is applied to find the variables that optimize the objective function(s), subject to the constraints. There is no theoretical limit to the capabilities of computational inverse approaches to provide quantitative inverse solutions, as long as the physical processes can be modeled computationally and there is the sensitivity with respect to the desired system features to be identified. Yet, for smart material shape changing structure applications, the use of these inverse methods have thus far been limited, and mainly seen in the design of shape memory alloy devices, particularly actuators [34, 71, 101]. In addition, one previous study by the authors [94] presented a proof-of-concept on using the computational inverse mechanics approach for the optimal design of morphing processes in locally activated smart material structures. The computational inverse mechanics approach was shown through numerical tests to provide a generalized and flexible means to facilitate the use of smart material structures to achieve desired morphing processes with controllable localized activation and actuation; however, the results were preliminary.

As discussed, there are three key components to be addressed for a typical computational inverse mechanics approach, the numerical representation, the objective function, and the optimization algorithm. Numerically representing the morphing process for a smart material structure accurately can be a potentially complicated process [20, 51, 56]. However, in terms of the inverse solution process, the numerical representation component is relatively straightforward, in that standard methods, such as finite element analysis, can often be employed, and the accuracy of this forward modeling has a clear and direct effect on the accuracy of the inverse solution. Alternatively, the issues of selecting an appropriate objective functional and optimization algorithm, which is the focus of the work herein, are intimately linked and have significantly less obvious implications. While much of the objective function and con-

straints are defined by the specifics of the application of interest, the specific form, such as the type of norm used (e.g., L_1 or L_2), affects the nature of the search space, and therefore, the ability of a particular optimization algorithm to traverse this search space to identify a solution estimate. Furthermore, depending on the optimization technique employed, other issues, such as differentiability of the objective and/or constraints may also need to be considered. In terms of the optimization algorithm selection, algorithms are often divided into two categories: non-gradient-based and gradient-based. Non-gradient-based algorithms, such as genetic algorithms [28, 72], which were used in the previous study by the authors [94], typically include some type of stochastic component in the search process to provide some degree of global search capabilities. Non-gradient-based algorithms are often easier to implement as well, being comparatively insensitive to the form of the objective functional and constraints. However, non-gradient-based algorithms can be prohibitively computationally expensive, requiring a comparatively large number of functional evaluations to estimate a solution. In contrast, gradient-based algorithms, such as Newton's methods [48, 49], can only be expected to converge to local solution estimates (unless the search space is convex, which is not often the case), but are computationally inexpensive, requiring substantially fewer function evaluations compared to non-gradient-based algorithms. In addition, gradient-based algorithms are not nearly as affected by the dimensionality of the problem (i.e., the number of system parameters to be determined), with most non-gradient-based algorithms becoming disproportionately more computationally expensive with increased problem dimensionality. It was noted in the previous study [94] that while the genetic algorithm provided a means to investigate the potential for computational design of smart material morphing structures as a proof-of-concept with the low-dimensional example cases considered therein, more significant and realistically applicable higher-dimensional examples would require a substantially more computationally efficient optimization approach to allow for a thorough investigation of the potential capabilities and to move towards potential implementation. Moreover, as is often the case with design or control-type inverse problems, many applications of the type of smart material morphing structure technology considered here would not require unique and/or (near)-global solutions, and a gradient-based optimization approach would be clearly preferable.

Naturally, the key to utilizing a gradient-based optimization method is to develop an approach to calculate the gradient of the objective functional with respect to the unknown parameters. One simple method to implement to approximate the gradient of the objective functional is to use a finite difference method. However, finite difference methods are limited in that they require the evaluation of the objective functional, which involves the solution of a computationally expensive boundary value problem in the case herein, a number of times on the order of the number of unknown parameters (e.g., $\mathbf{N} + \mathbf{1}$ for forward or backward finite difference methods, where \mathbf{N} is the number of design parameters to be determined). Direct differentiation of the objective functional can improve the accuracy of the gradient calculation compared to finite difference, but does not necessarily improve the computational expense, requiring \mathbf{N} evaluations of the differentiated boundary value problems, and is considerably more difficult to implement. Generally, for problems with even a moderately large number of unknown design parameters to be determined, both finite difference and direct differentiation can be computationally prohibitive. Alternatively, adjoint methods, which have seen increasing use in a variety of computational inverse mechanics applications, are capable of evaluating the gradient of an objective functional involving a boundary value problem with a cost equivalent to only $\mathbf{2}$ boundary value problem evaluations, regardless of the number of design parameters \mathbf{N} . While substantially more computationally efficient than the other two techniques, one particular challenge of adjoint methods is that they require the derivation and implementation of an adjoint boundary value problem. Applications of computational inverse mechanics using the adjoint method have included characterization and design/control problems in elasticity [6], electromagnetics [25], aerodynamics [45], acoustics [32], and heat conduction [114], among others.

The current work presents an efficient computational inverse mechanics strategy using the adjoint method for the design or control of locally activated and actuated smart material morphing structures. This work extends the previous proof-of-concept study to not only address computational efficiency, but to also further explore the potential capabilities of this smart material structure concept to achieve diverse morphing targets with energy efficiency through controllable distributed activation and actuation. As previously, for simplicity, the present study focused on thermally responsive SMP, but the approach is generalizable to a

wide variety of smart materials, design objectives, and constraints. The general computational inverse problem solution approach for the design or control of smart material morphing structures is presented in Section 2.3. The forward boundary value problem describing the morphing process of a thermally responsive smart material structure given a prescribed activation and actuation and the algorithm to determine the optimal activation and actuation parameters to achieve a desired morphing process based on the adjoint method are presented in Sections 2.4 and 2.5, respectively. Then, two design/control example problems of skeletal structural components are presented in Section 2.6 to show the capabilities of the proposed approach, which is followed by the concluding remarks in Section 2.7.

2.3 COMPUTATIONAL DESIGN/CONTROL FRAMEWORK FOR MORPHING STRUCTURES

The general active morphing concept considered in this work for a structure composed of thermally responsive smart materials followed the same overall format as the previous study [94]. In this concept, the morphing process begins with some portion of the domain heated with a controllable transient temperature distribution and/or surface heat flux ($T^A(\vec{x}, t)$ or $q^A(\vec{x}, t)$). Once a sufficient portion of the structure is softened through activation, mechanical actuation begins through controlled transient displacement and/or force ($\vec{u}^A(\vec{x}, t)$ or $\vec{r}^A(\vec{x}, t)$) to deform the structure into a desired shape. Therefore, the design/control problem to identify the activation and actuation distributions to achieve the desired shape change can be cast in a general way in the form of the following constrained optimization problem:

$$\text{Minimize : } \left\{ \begin{array}{l} \| s^{target} - s^{approx}(T^A, q^A, \vec{u}^A, \vec{r}^A) \|_{\Omega, t_F} \\ J_T(T^A, q^A, \vec{u}^A, \vec{r}^A) \\ J_W(T^A, q^A, \vec{u}^A, \vec{r}^A) \\ t_F(T^A, q^A, \vec{u}^A, \vec{r}^A) \\ w(T^A, q^A, \vec{u}^A, \vec{r}^A) \end{array} \right. \quad (2.1)$$

$$\text{Subject to : } \left\{ \begin{array}{l} \tilde{\sigma}(\boldsymbol{\sigma}(\vec{x}, t; T^A, q^A, \vec{u}^A, \vec{r}^A)) < \sigma^{damage}, \quad \forall \vec{x} \in \Omega, \quad t \in [0, t_F] \\ T(\vec{x}, t; T^A, q^A, \vec{u}^A, \vec{r}^A) < T^{damage}, \quad \forall \vec{x} \in \Omega, \quad t \in [0, t_F] \end{array} \right. \quad (2.2)$$

where \vec{x} is the spatial position vector, t is the time, Ω is the spatial domain of the structure, t_F is the total time of the morphing process, $\|\cdot\|_{\Omega,t_F}$ is the metric norm with respect to the spatial domain and time, s^{target} is the desired shape change, s^{approx} is the approximate expected shape change given the design parameters predicted by a numerical representation of the structure, J_T and J_W are the total thermal energy and mechanical work, respectively, predicted by the numerical representation to perform the morph, w represents additional design objectives that may be desired, σ and T are the approximate expected internal stress tensor and internal temperature, respectively, predicted by the numerical representation throughout the structure during the morphing process, $\tilde{\sigma}(\cdot)$ is a suitable scalar stress transform (e.g., von Mises criterion), and σ^{damage} and T^{damage} are the stress and temperature limits, respectively, to avoid damaging the material. As discussed in the Introduction, the constrained optimization problem (Eqns. 2.1 - 2.2) will be solved through a computational inverse problem solution approach that combines a numerical representation of the morphing system (i.e., forward problem) and a nonlinear optimization strategy to identify the parameters that minimize the desired objectives while satisfying the required constraints, as detailed in the following.

2.4 FORWARD PROBLEM

The structures considered here were assumed to be composed entirely of thermally responsive SMP subject only to applied thermal activation and mechanical actuation. At the continuum level the nonlinear coupled thermo-mechanical behavior of smart materials can be theoretically described by the conservation of mass, linear and angular momentum, and energy. However, for simplicity the activation process was assumed to occur entirely through a temperature-dependent Young's modulus, and the behavior of the structures was assumed to be defined by linear transient heat transfer and linear elastic quasi-static solid mechanics. Therefore, the only thermo-mechanical coupling was assumed to be with respect to the Young's modulus, and all morphing processes were simulated with sequentially coupled thermo-mechanical analyses (i.e., uncoupled thermal analysis sequentially followed by

a temperature-dependent mechanical analysis). While these simplifications are noted to be significant and would not be expected to be sufficient for accurately modeling the finite strain nonlinear thermo-mechanical behavior of SMP structures, the relative overall behavior should not depend significantly on the simplifications applied herein. Furthermore, tests were performed throughout the previous studies comparing the pure linear model with a simple nonlinear hyperelastic model, which showed that although there were differences in the stresses occurring during the morphing process for the two models, the relative overall stress distributions remained nearly identical and the behaviors predicted using the linear models were generally conservative. Therefore, the morphing process of a smart material structure for the present work was represented by the following initial boundary value problem:

$$k\nabla^2 T(\vec{x}, t) = \rho c \frac{\partial T(\vec{x}, t)}{\partial t}, \quad \forall \vec{x} \in \Omega, t \in [0, t_F], \quad (2.3)$$

$$\nabla \cdot \boldsymbol{\sigma}(\vec{x}, t) = \vec{0}, \quad \forall \vec{x} \in \Omega, t \in [0, t_F], \quad (2.4)$$

$$T(\vec{x}, 0) = T_0, \quad \forall \vec{x} \in \Omega, t = 0, \quad (2.5)$$

$$T(\vec{x}, t) = T^A(\vec{x}, t), \quad \forall \vec{x} \in \Gamma_T, t \in [0, t_F], \quad (2.6)$$

$$-k\nabla T(\vec{x}, t) \cdot \vec{n}(\vec{x}) = q^A, \quad \forall \vec{x} \in \Gamma_q, t \in [0, t_F], \quad (2.7)$$

$$\vec{u}(\vec{x}, t) = \vec{u}^A(\vec{x}, t), \quad \forall \vec{x} \in \Gamma_U, t \in [0, t_F], \quad (2.8)$$

$$\boldsymbol{\sigma}(\vec{x}, t) \cdot \vec{n}(\vec{x}) = \vec{\tau}^A(\vec{x}, t), \quad \forall \vec{x} \in \Gamma_{\vec{\tau}}, t \in [0, t_F], \quad (2.9)$$

$$\boldsymbol{\sigma}(\vec{x}, t) = \mathbf{C}^{IV}(E(T), \nu) : \boldsymbol{\epsilon}(\vec{x}, t), \quad \forall \vec{x} \in \Omega, t \in [0, t_F], \quad (2.10)$$

$$\boldsymbol{\epsilon}(\vec{x}, t) = \frac{1}{2}[\nabla \vec{u}(\vec{x}, t) + \nabla \vec{u}(\vec{x}, t)^T], \quad \forall \vec{x} \in \Omega, t \in [0, t_F], \quad (2.11)$$

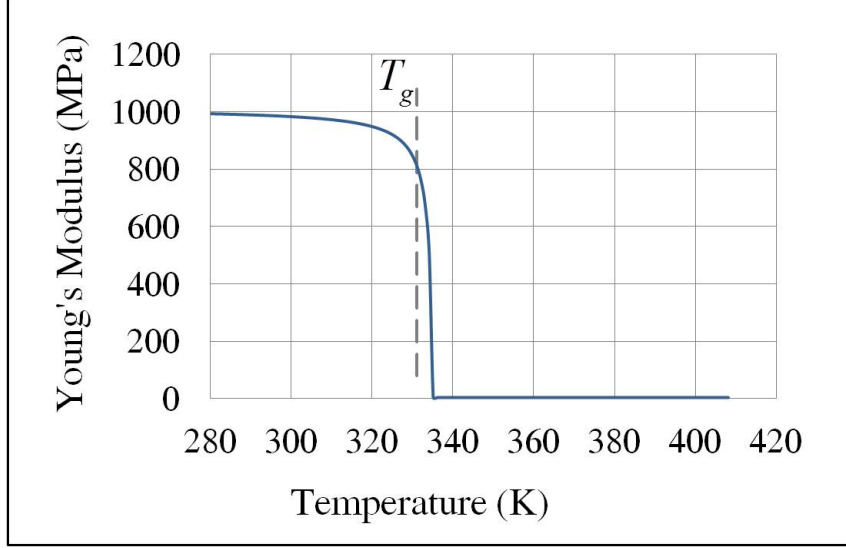


Figure 2.1: The assumed relationship between Young's modulus and temperature for the numerical study

where k is the thermal conductivity, ρ is the mass density, c is the specific heat, $\boldsymbol{\sigma}$ is the Cauchy stress tensor, $\boldsymbol{\epsilon}$ is the small strain tensor, \mathbf{C}^{IV} is the fourth order elastic stiffness tensor, E is the Young's modulus, ν is the Poisson's ratio, \vec{u} is the displacement vector, Ω is the spatial domain, Γ is the domain boundary, \vec{n} is the unit outward normal vector on the boundary. Γ_T is the portion of the domain boundary where the temperature is specified, Γ_q is the portion of the domain boundary where the heat flux is specified, Γ_U is the portion of the domain boundary where the displacement is specified, and $\Gamma_{\vec{\tau}}$ is the portion of the domain boundary where the traction is specified.

The chosen material parameters were based on those published for the commercially available thermally responsive SMP Veriflex [15, 44, 53, 62]. Figure 2.1 shows the assumed relationship between the elastic modulus and temperature, with the modulus varying between 1050MPa in the glassy state to 0.24MPa in the rubbery state when heated above the glass transition temperature ($T_g = 62^\circ\text{C}$ or 335.15K). The remaining mechanical and thermal material parameters are shown in Table 2.1.

Table 2.1: The assumed material parameters for the numerical study.

Material Parameter	Value
Poisson's ratio	0.45
Density	$920kg/(m^3)$
Specific heat	$1800J/(kg \cdot K)$
Thermal conductivity	$0.17W/(m \cdot K)$
Convective heat transfer coefficient	$25W/(m^2 \cdot K)$

2.5 OPTIMIZATION OBJECTIVES AND SOLUTION ALGORITHM

The design/control objectives for the present study were assumed to be minimizing the total energy of the morphing process ($J = J_T + J_W$) and/or achieving a desired shape change by minimizing a measure of morphing error (S). Based on the forward model formulated in Section 2.4, the total thermal energy (J_T) required for activation and the total mechanical work (J_W) required for actuation can be determined, respectively, through:

$$J_T = \int_t \int_{\Omega} \rho c [T(\vec{x}, t) - T_0] \delta(t - t_F) d\vec{x} dt \quad (2.12)$$

and

$$J_W = \int_t \int_{\Gamma} \boldsymbol{\sigma}(\vec{x}, t) \cdot \vec{n}(\vec{x}) \cdot \vec{u}(\vec{x}, t) d\vec{x} dt, \quad (2.13)$$

where δ is the Dirac delta function. In addition, the morphing error was defined as the difference between a desired displacement field and the displacement field predicted by the forward problem simulation at the completion of the morphing process, as:

$$S = \int_t \int_{\Omega} \sum_{m=1}^M [\vec{u}(\vec{x}, t) - \vec{u}^{target}(\vec{x}, t)]^2 \delta(\vec{x} - \vec{x}_m^*) \delta(t - t_F) d\vec{x} dt, \quad (2.14)$$

where \vec{u} and \vec{u}^{target} are the predicted and desired (i.e., target) displacement fields, respectively, $\{\vec{x}_m^*\}_{m=1}^M$ is the set of M discrete spatial locations where the target displacement is

desired to be achieved by the morph, and t_F is the time at the completion of the morphing process. Although addressing both the energy and morphing error constitutes a multi-objective optimization problem, as is commonly done, for the present work the multi-objective optimization problem was transformed into a single objective problem by simply using a weighted sum of the two objectives. As such, the final objective function for the design/control optimization utilized herein can be shown as:

$$f(\vec{p}) = J(\vec{p}) + C \cdot S(\vec{p}) \quad (2.15)$$

where \vec{p} is the vector of unknown design parameters to be determined through the optimization (i.e., activation and actuation parameters) and C is the scalar weighting constant (note that the specific value of the weighting constant allows emphasis of the optimization effort to be placed on a specific objective, energy or shape, depending on the relative importance for a particular application).

While a genetic algorithm (as used in [94]) was applied to a portion of the examples considered herein to serve as a basis of comparison, the focus of the present work is on computational efficiency through gradient-based optimization, particularly relying on the adjoint approach to expedite gradient calculations, for the minimization of Eqn. 2.15. A quasi-Newton gradient-based algorithm, the BFGS interior point algorithm [3, 61, 86], was chosen for this purpose, and the details of the adjoint approach to calculate the gradient of the objective function (f) with respect to the design parameters (\vec{p}) to drive this gradient-based optimization process are presented in the following.

2.5.1 Gradient Calculation using the Adjoint Method

The overall key to the adjoint method is the formulation of an adjoint (initial boundary value) problem in terms of a set of Lagrange multipliers that is derived from the objective functional(s) and the associated forward boundary value problem(s). The first step in this approach is to form the Lagrangian, in which the inner product is taken between a Lagrange

multiplier and each governing equation of the forward initial boundary value problem(s) (Eqns. 2.3 and 2.4). It is then added to the objective functional(s) (Eqn. 2.15), to obtain:

$$L(\vec{p}) = f(\vec{p}) + \int_t \int_{\Omega} \left[\lambda(\vec{x}, t, \vec{p}) \cdot g(\vec{x}, t, \vec{p}) + \vec{\varphi}(\vec{x}, t, \vec{p}) \cdot \vec{h}(\vec{x}, t, \vec{p}) \right] d\vec{x} dt. \quad (2.16)$$

where for the present work g and \vec{h} are the governing equations for heat transfer (Eqn. 2.3) and solid mechanics (Eqn. 2.4), respectively, λ is the Lagrange multiplier associated with the heat transfer problem and $\vec{\varphi}$ is the Lagrange multiplier vector associated with the solid mechanics problem. Since the governing equations are satisfied everywhere in the domain (i.e., $g(\vec{x}, t, \vec{p}) = 0$ and $\vec{h}(\vec{x}, t, \vec{p}) = \vec{0}$, $\forall \vec{x} \in \Omega$), the Lagrangian is equivalent to the objective function for any arbitrary set of Lagrange multipliers. Thus, the gradient of the Lagrangian is also equivalent to the gradient of the objective function, which can be written for the j^{th} design parameter as:

$$\frac{dL}{dp_j} = \frac{\partial f}{\partial p_j} + \int_t \int_{\Omega} \left[\lambda \frac{\partial g}{\partial p_j} + \vec{\varphi} \cdot \frac{\partial \vec{h}}{\partial p_j} \right] d\vec{x} dt. \quad (2.17)$$

After expanding and manipulating Eqn. 2.17, each term that multiplies the temperature and displacement gradients ($\frac{\partial T}{\partial p_j}$ and $\frac{\partial \vec{u}}{\partial p_j}$) is set to zero (to avoid calculation of these undesirable terms without loss of generality since the Lagrange multipliers are arbitrary) to produce the following adjoint problem for the Lagrange multipliers:

$$k \nabla^2 \lambda(\vec{x}, t) + \rho c \frac{\partial \lambda(\vec{x}, t)}{\partial t} - \frac{1}{E} \frac{\partial E}{\partial T} (\nabla \vec{\varphi}) : \boldsymbol{\sigma}_{\vec{u}} = 0, \quad \forall \vec{x} \in \Omega, t \in [0, t_F], \quad (2.18)$$

$$\nabla \cdot \boldsymbol{\sigma}_{\vec{\varphi}}(\vec{x}, t) + C \sum_{m=1}^M 2[\vec{u} - \vec{u}^{target}] \delta(\vec{x} - \vec{x}_m^*) \delta(t - t_F) = \vec{0}, \quad \forall \vec{x} \in \Omega, t \in [0, t_F], \quad (2.19)$$

$$\lambda(\vec{x}, t_F) = 0, \quad \forall \vec{x} \in \Omega, t = t_F, \quad (2.20)$$

$$\lambda(\vec{x}, t) = 0, \quad \forall \vec{x} \in \Gamma_T, t \in [0, t_F], \quad (2.21)$$

$$-k \nabla \lambda(\vec{x}, t) \cdot \vec{n}(\vec{x}) = 0, \quad \forall \vec{x} \in \Gamma_q, t \in [0, t_F], \quad (2.22)$$

$$\vec{\varphi}(\vec{x}, t) = -\vec{u}^A(\vec{x}, t), \quad \forall \vec{x} \in \Gamma_U, t \in [0, t_F], \quad (2.23)$$

$$\boldsymbol{\sigma}_{\vec{\varphi}}(\vec{x}, t) \cdot \vec{n}(\vec{x}) - \vec{\tau}^A \delta(t - t_F) + \frac{\partial \vec{\tau}^A}{\partial t} = \vec{0}, \quad \forall \vec{x} \in \Gamma_{\vec{\tau}}, t \in [0, t_F], \quad (2.24)$$

Therefore, after solving the above adjoint problem for the Lagrange multipliers, the gradient of the Lagrangian, and by extension, the gradient of the objective function can be calculated as:

$$\begin{aligned} \frac{dL}{dp_j} = & \int_t \int_{\Gamma_T} (-k \nabla \lambda \cdot \vec{n}) \frac{\partial T^A}{\partial p_j} d\vec{x} dt - \int_t \int_{\Gamma_q} \left(\lambda \frac{\partial q^A}{\partial p_j} \right) d\vec{x} dt \\ & + \int_t \int_{\Gamma_{\vec{\tau}}} \left(\vec{\varphi} + \vec{u}^A \right) \frac{\partial \vec{\tau}^A}{\partial p_j} d\vec{x} dt + \int_t \int_{\Gamma_U} \left(-\boldsymbol{\sigma}_{\vec{\varphi}} \cdot \vec{n} \cdot \frac{\partial \vec{u}^A}{\partial p_j} + \boldsymbol{\sigma}_{\vec{u}} \cdot \vec{n} \cdot \frac{\partial \vec{u}^A}{\partial p_j} \right) d\vec{x} dt, \end{aligned} \quad (2.25)$$

where

$$\boldsymbol{\sigma}_{\vec{u}} = \frac{E}{2(1+\nu)} [\nabla \vec{u} + \nabla(\vec{u})^T] + \frac{E}{(1+\nu)(1-2\nu)} (\nabla \cdot \vec{u}) \mathbf{I} \quad (2.26)$$

and

$$\boldsymbol{\sigma}_{\vec{\varphi}} = \frac{E}{2(1+\nu)} [\nabla \vec{\varphi} + \nabla(\vec{\varphi})^T] + \frac{E}{(1+\nu)(1-2\nu)} (\nabla \cdot \vec{\varphi}) \mathbf{I}, \quad (2.27)$$

and \mathbf{I} is the identity tensor.

In summary, the algorithm for the calculation of the gradient using the adjoint method can be summarized as follows:

- (1) Solve the forward initial boundary value problem (Eqns. 2.3 - 2.11) to obtain the displacement field \vec{u} and the temperature field T .
- (2) Solve the adjoint initial boundary value problem (Eqns. 2.18 - 2.24) to obtain the Lagrange multipliers λ and $\vec{\varphi}$.
- (3) Substitute \vec{u} , T , λ and $\vec{\varphi}$ into Eqn. 2.25 to compute the gradient of the objective function.

Similar to the forward initial boundary value problem, in the present work the adjoint problem was solved using the traditional Galerkin finite element method. An additional note of interest is that the adjoint problem (Eqns. 2.18 - 2.24) is of the same form as the forward problem (Eqns. 2.3 - 2.11), but is driven/forced by the components of the objective function (i.e., the energy and morphing objective functions). Furthermore, the adjoint problem has conditions specified at the final time, rather than the initial time, and the sequential coupling is reversed compared to the forward problem, with the temperature Lagrange multiplier being dependent upon the displacement Lagrange multiplier, whereas in the forward problem displacement is dependent upon temperature.

2.6 NUMERICAL INVESTIGATION

To test the inherent benefits and challenges of the proposed computational approach using the adjoint method, a numerical investigation was performed with example design applications from concepts of morphing skeletal structural components (i.e., framing and connecting elements). First, a smart link concept with direct shape control was tested to verify the computational framework, as well as to compare the efficiency and effectiveness of the computational approach using the adjoint method with a non-gradient-based approach (a genetic algorithm in this case). Lastly, an example of a morphing structural backbone with substantially increased complexity of design parameters and objectives compared to the first example was considered. This second example was intended to more thoroughly explore the capabilities of the design/control approach presented with multiple locally activated and actuated smart material structures to uniquely facilitate complex morphing capabilities, in terms of complex target shapes, multiple morphing targets from fixed instrumentation, and indirectly controlled target shape changes.

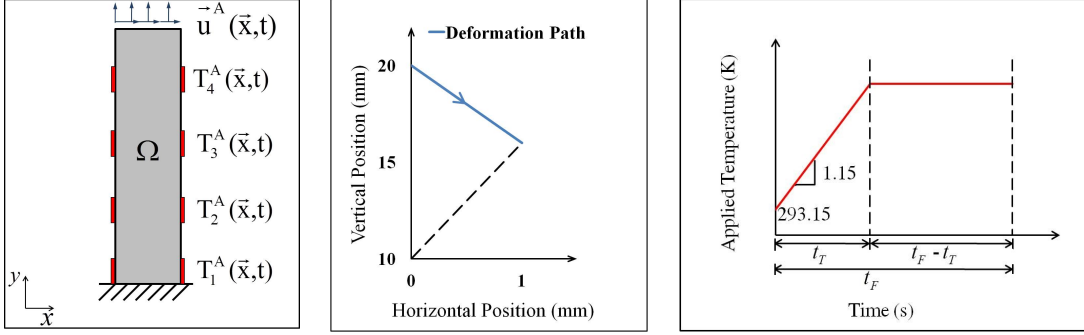


Figure 2.2: (a) Schematic of the smart link design concept, (b) the deformation path considered for the top of the structure, and (c) the applied temperature with respect to time for Example 1: Smart Link.

2.6.1 Example 1: Smart Link

The concept of a smart structural link considered here implies a structural element that connects other components of a structural frame, which is capable of changing the shape of the structure by changing the positioning of the connected elements through morphing of the link (e.g., [62]). The optimal local activation and actuation design approach here seeks to create a design for the activation and actuation process of the link with considerable savings in both time and energy required to morph the structural component and is compared to a more standard implementation strategy (i.e., full activation). As shown in Figure 2.2, a $20\text{mm} \times 5\text{mm} \times 1\text{mm}$ homogeneous rectangular prism composed of thermally responsive SMP was considered and analyzed using the plane stress assumption (note that the size was reduced with respect to in-use structures to reduce computing costs, but the observations with respect to the inverse procedure should not be significantly affected by the size of the structure). The morphing procedure considered involved first heating the structure in its cast configuration to initiate the activation process. After some time of purely heating, actuation would be applied to deform the structure into the desired shape. As such, the total time to perform the structural morphing, t_F , was simply the summation of the purely heating time prior to actuation, t_D , and the actuation time, t_M .

Table 2.2: Applied displacement boundary conditions for Example 1: Smart Link.

	$0 \leq t \leq t_D$	$t_D \leq t \leq t_F$
Fixed boundary	$u_1^A(\vec{x}, t) = 0$	$u_1^A(\vec{x}, t) = 0$
	$u_2^A(\vec{x}, t) = 0$	$u_2^A(\vec{x}, t) = 0$
Actuated boundary	$u_1^A(\vec{x}, t) = 0$	$u_1^A(\vec{x}, t) = \frac{u_1^{target}}{t_M} \cdot (t - t_D)$
	$u_2^A(\vec{x}, t) = 0$	$u_2^A(\vec{x}, t) = \frac{u_2^{target}}{t_M} \cdot (t - t_D)$

For the mechanical actuation process the bottom of the structure was assumed to be fixed to a rigid support and the displacement across the top of the structure was uniformly controlled to meet the target deformation (i.e., actuation was applied only to the top surface, and the target shape change only considered the top surface). In addition, actuation was assumed to occur at a constant rate. Therefore, the actuation process could be defined by the target displacement, \vec{u}^{target} , the purely heating time prior to actuation, t_D , and the actuation time, t_M , as shown in terms of the displacement boundary conditions in Table 2.2.

The remaining boundaries were taken to be traction free. Note that the desired shape change/deformation in this example problem was directly controlled, and was not a design variable. Figure 2.2 shows the controlled deformation path for each point across the top surface of the structure.

For the thermal activation process the entire structure was assumed to be initially at room temperature ($293K$) and the applied temperature was assumed to be controllable with four symmetric pairs of 20mm long heating pads along both sides of the link starting from the fixed support and separated by 30mm along the height of the link, as shown in Figure 2.2. Temperature was assumed to be applied uniformly throughout the length of each heating pad and to increase linearly in time on that region starting from room temperature at a fixed rate of $1.15K/s$ for a controllable “warm-up” duration, t_T , and then held constant until morphing was completed, as shown in Figure 2.2. The portion of the boundary not being heated was assumed to be insulated.

Table 2.3: Summary of the optimization objective and constraints for Example 1: Smart Link.

Objective Function	$f = J = J_T + J_W$
Design Parameters	$0 < t_T^i \leq 100s, \quad \text{for } i = 1, 2, 3, 4$
and Constraints	$\ \sigma^{von} \ _{L^\infty(\Omega)} \leq 11.5MPa$

For this first example a single design objective was used, which was to minimize the total combined energy (i.e., the sum of Eqns. 2.12 and 2.13). The constraints included the maximum temperature to prevent damage of $408K$, which was implemented by constraining the warm-up time for each heating pad (t_T^i for $i = 1, 2, 3, 4$) to a maximum of $100s$, and the maximum von Mises stress ($\| \sigma^{von} \|_{L^\infty(\Omega)}$) to prevent damage of $11.5MPa$. The potential design variables initially considered for optimizing the design of the thermal activation and mechanical actuation included the warm-up time for each pair of heating pads, the heating time prior to actuation, and the actuation time. However, after performing a sensitivity analysis, the effect of the heating time prior to actuation and the actuation time on the morphing process outcome were found to be minimal (with respect to the minimum values) in comparison to the warm-up times. Therefore, the chosen design variables to be determined for this example were the warm-up time for each symmetric pair of heating pads, such that $\vec{p} = [t_T^1, t_T^2, t_T^3, t_T^4]$, and the heating time prior to actuation and the actuation time were fixed at values of $t_D = 290s$ and $t_M = 10s$.

Table 2.3 shows a summary of the constrained optimization problem constructed for this first example. As stated previously, to examine the benefits and challenges of the presented computational design/control approach using a gradient-based optimization algorithm with the adjoint method, a non-gradient-based genetic algorithm (GA) was also applied to solve the constrained optimization problem to provide a point of comparison. An additional solution procedure note is that the gradient-based optimization was applied 10 times with

randomly selected “initial” parameter vector values, and the best result from this set of 10 solution estimates was chosen as the “final” estimate of the gradient-based optimization procedure. This type of “multi-start” gradient-based optimization procedure is a relatively common approach to try to overcome some of the local search limitations of gradient-based optimization, while not eliminating the computational efficiency benefits. Note that the adjoint implementation was also verified by repeating the gradient-based optimization process with a finite difference approximation of the gradient (which was feasible due to the low-dimensionality of this first example), and the two approaches were found to produce equivalent results (not shown here for brevity). The stopping criteria for the optimization processes (both gradient- and non-gradient-based) was set to be a relative change in the objective function value of 0.005% in subsequent iterations. To provide a point of reference for both optimization procedures, a “control” design was established resembling the current standard of practice for such a smart link concept, in which actuation was applied to deform the structure only after the entire volume of the structure was activated (i.e., the entire domain temperature reached a value greater than T_g).

2.6.1.1 Results and Discussion: To show the nature of the optimal design results, Figure 2.3 shows an example of the temperature field at initiation of morphing and the stress distribution and the final deformed shape of the optimized design using the gradient-based algorithm with the adjoint method.

As can be seen from the representative example, the optimized design solutions had a maximum von Mises stress during the morphing process very near to the stress limit (i.e., damage stress). Furthermore, the thermal energy dominated the energy consumption of the morphing process, thus, the primary objective of the optimization naturally became identifying the applied heating to minimally activate the structure to prevent damage during the morph. More importantly, Table 2.4 shows the control design parameters, the optimized design parameters from the GA optimization, and the optimized design parameters from the gradient-based optimization using the adjoint method, along with the corresponding activation thermal energy (J_T), actuation mechanical work (J_W), and total energy (J), and the percent difference for these energies with respect to the control design. The GA

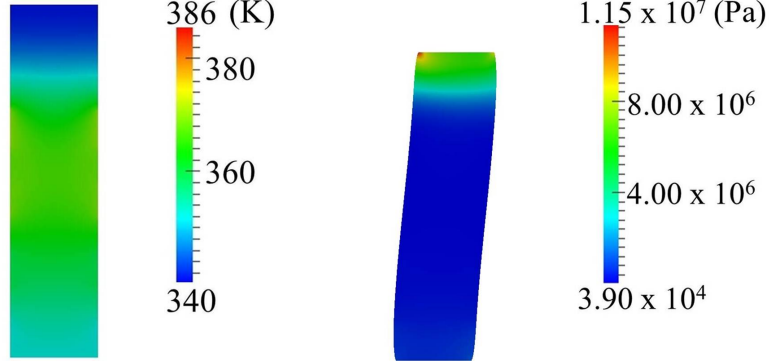


Figure 2.3: (a) Temperature distribution at initiation of morphing and (b) stress distribution and final deformed shape from optimized design solution from gradient-based optimization using the adjoint method for Example 1: Smart Link.

Table 2.4: Control, optimized design parameters from Genetic Algorithm optimization (GA Opt), optimized design parameters from quasi-Newton gradient-based optimization using the adjoint method (Adjoint Opt), resulting energy consumption to perform the morph, and the percent difference (%Diff) with respect to the control design for Example 1: Smart Link ($mJ = 10^{-3} \text{Joule}$).

Design	t_T^1	t_T^2	t_T^3	t_T^4	J_T	J_W	J
Case	(s)	(s)	(s)	(s)	(mJ)	(mJ)	(mJ)
Control	80.0	80.0	80.0	80.0	14037.5	10.4	14047.9
GA Opt	44.4	42.5	41.5	69.3	9231.2	83.2	9314.5
%Diff	-44.5	-46.9	-48.2	-13.3	-34.2	+704.0	-33.7
Adjoint Opt	51.0	57.3	65.6	66.7	10833.9	86.7	10920.6
%Diff	-36.2	-28.4	-18.0	-16.6	-22.8	+737.1	-22.3

results represent an approximation of the best possible results that could be obtained from the computational design procedure, yielding an energy savings of more than 30% with respect to the control design, but required an extensive computational cost, on the order of 10^4 function evaluations, to achieve convergence. Again, note that with even a relatively small increase in complexity, and therefore, computational cost per function evaluation of the morphing system, the amount of evaluations required by the GA to converge would be infeasible. Alternatively, the gradient-based optimization results were able to yield less energy savings than the GA, but still a substantial amount at over 20% with respect to the control design, but required two orders of magnitude less function evaluations, on the order of 10^2 , than the GA to achieve convergence (even with the 10 runs with different initial parameter sets). Furthermore, it is often the case for design or control problems such as this that an approximation of the global minimum is unnecessary, and a local solution would be sufficient. In such instances, the substantial improvement in computational savings provided by the gradient-based approach with the adjoint method would likely outweigh the loss in global search capabilities.

2.6.2 Example 2: Morphing Structural Backbone

The concept of a morphing structural backbone considered here implies a structural element that is directly connected to the exposed surface of the structure, and therefore, the overall shape of the backbone, not just the positioning of the endpoints, affects the function of the structure. For example, this type of morphing component could be installed in the edge of an aerodynamic structure, for which it may be desirable to use the component to prescribe both the size as well as the shape of all or some part of the structure's surface. A schematic of the structural backbone considered for this second example is shown in Figure 2.4. The structure was taken to be a homogeneous half-circular prism with a 150mm outer radius composed of thermally responsive SMP, and the structure was analyzed using the plane strain assumption.

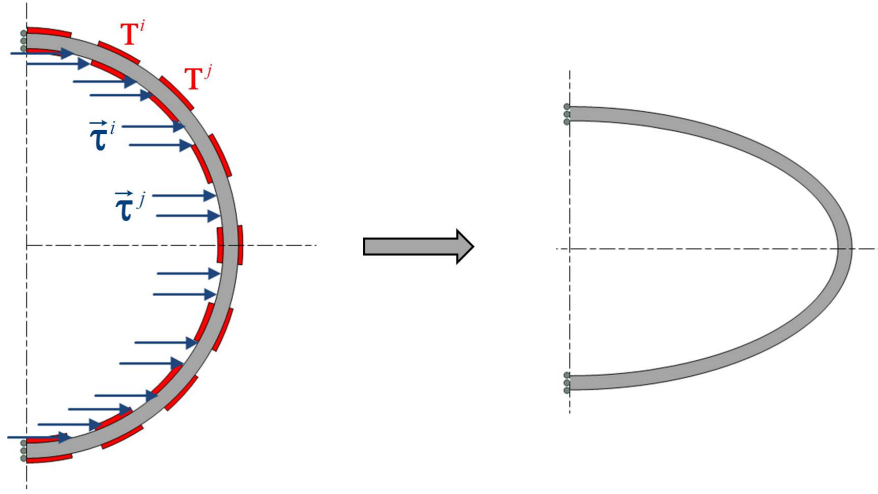


Figure 2.4: Schematic of the Morphing Structural Backbone Design Concept for Example 2.

The morphing procedure applied followed a similar sequencing pattern as the first example. However, to provide greater degrees of freedom for the design/control of the morphing system, several more heating pads and actuators were employed in this case compared to the first example, with a total of nine pairs of approximately 45mm long heating pads (i.e., 18 total heating pads) and eight approximately 15mm long actuation regions, all equally spaced along the surface of the structure. Additionally, the operation of the structure and the design/control objectives were assumed to be symmetric with respect to the horizontal axis. Thus, only the top half to the structure needed to be analyzed and the morphing process of the structure was defined by 10 independent heating pads and four actuators (note that the heating pad pairs were not linked in this example as was the case in the first example). For the thermal activation process the entire structure was assumed to be initially at room temperature (293K), and the 10 heating pads along the outer and inner surface of the structure were heated independently (i.e., prescribing a different t_T^i for each heating pad) following the same heating pattern as was used in the first example problem (shown in Figure 2.2). For the mechanical actuation process the two ends of the structure were assumed to be constrained in the horizontal direction and the amplitude of the horizontal

Table 2.5: Applied traction boundary conditions for Example 2: Morphing Structural Backbone.

	$0 \leq t \leq t_D$	$t_D \leq t \leq t_F$
	$\tau_1^A(\vec{x}, t) = 0$	$\tau_1^A(\vec{x}, t) = \frac{\tau_1^i}{t_M} \cdot (t - t_D)$
Actuated Boundary $\{\Gamma_{\vec{\tau}}^i\}_{i=1}^4$	$\tau_2^A(\vec{x}, t) = 0$	$\tau_2^A(\vec{x}, t) = 0$

tractions (τ_1^i) over each actuation region was controllable and assumed to increase linearly in time to deform the structure, while the remaining boundaries were taken to be traction free. The actuator traction boundary conditions that were applied uniformly over the length of each actuation region are described in Table 2.5.

Similarly to the previous example, neither the time to complete the deformation nor the heating time prior to actuation had a significant effect on the design objectives, and were again fixed at values of $t_M = 10s$ and $t_D = 590s$. Therefore, the chosen design variables to be determined in this example were the warm-up time for each heating pad and the maximum amplitude of the actuation force, such that $\vec{p} = [t_T^1, t_T^2, \dots, t_T^{10}, \tau_1^1, \tau_1^2, \tau_1^3, \tau_1^4]$.

The overall optimal design/control objective of this second example was to identify the multiple activation and actuation parameters to minimize both the total energy of the morphing process and the morphing error (Eqn. 2.15). Table 2.6 shows a summary of the constrained optimization problem constructed for this morphing structural backbone example. For this example, only the gradient-based optimization algorithm with the adjoint method was applied, again with 10 randomly selected initial parameter vector values and selecting the best result from these 10 outcomes, and using the same stopping criteria as the previous example. Firstly, to explore the capabilities of the computational design/control approach for this morphing structural backbone system with the increased complexity of the design parameters, a relatively simple elliptical target shape (as shown in Figure 2.4) was considered. In particular, to better understand the tradeoff between the energy objective and the morphing error objective, a variety of different weightings was considered for the

Table 2.6: Summary of the optimization objective and constraints for Example 2: Morphing Structural Backbone.

Objective Function	$f = J + C \cdot S$
Design Parameters	$0 < t_T^i \leq 100s, (i = 1, 2, 3 \dots 10.)$
and Constraints	$0 < \tau_1^i \leq 0.1MPa, (i = 1, 2, 3, 4.)$
	$\ \sigma^{von} \ _{L^\infty(\Omega)} \leq 11.5MPa$

two objectives with the optimization process repeated for each weight value considered with $C \in [10^3, 10^5]$. Then, to further explore the ability of the proposed computational approach to facilitate smart material structures with multiple controllable localized activations and actuations to achieve complex morphing capabilities, a set of substantially more complex shape targets was considered (e.g., square and step-type target shapes).

2.6.2.1 Results and Discussion: Figure 2.5 shows the separate objective function values (i.e., total energy and morphing error) for a representative set of three of the optimal design solutions for the elliptical target shape corresponding to varying objective function weight values (C).

Overall, all optimal designs were able to relatively accurately achieve the targeted elliptical shape, substantially reducing the morphing error from the starting shape (i.e. the shape prior to applying any actuation) value of $S_0 = 0.38$ by more than 90%. However, there was clearly a significant tradeoff between the achievable energy savings and the morphing error. For the highest weighting parameter value (i.e., more emphasis placed on the morphing error) the required energy to achieve the morphing was approximately twice the energy than was required with the lowest weighting parameter value. The morphing error also changes by approximately a factor of 2 based on the weighting parameter values, but since all designs achieved what could be considered an accurate shape change, for this shape

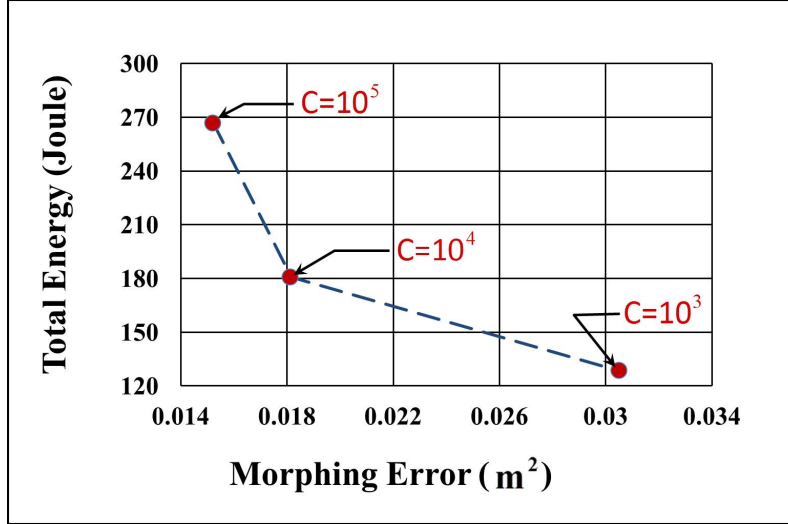
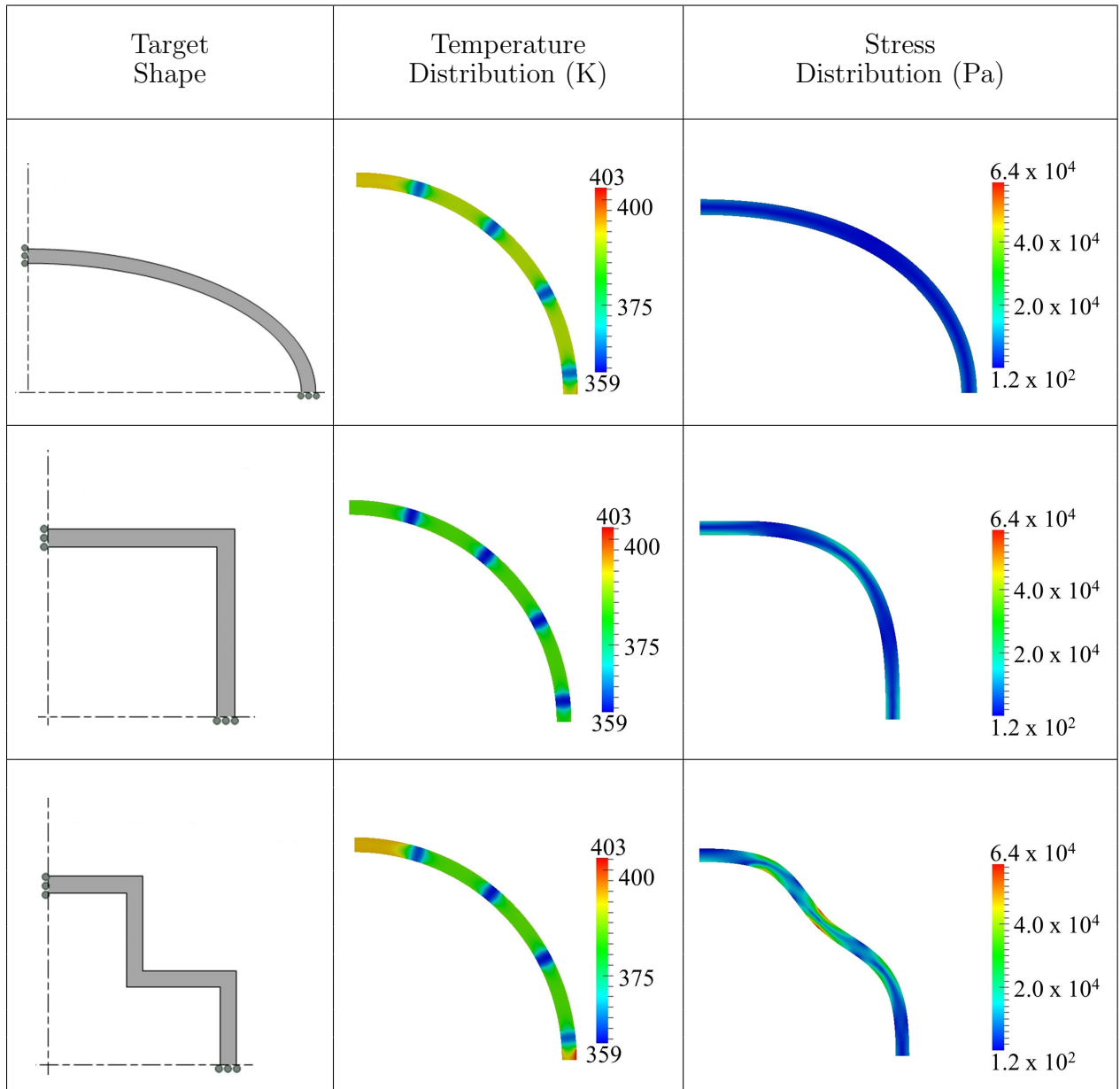


Figure 2.5: Total energy consumption (J) and morphing error (S) for three optimized design solutions with varying weighting parameters (C) for the elliptic target shape for Example 2: Morphing Structural Backbone.

target an emphasis on energy savings would likely be preferred. It should be noted that the minimum and maximum weighting parameter value results shown represent approximately the two extremes of the two-objective designs (i.e., the maximum emphasis on the energy and the maximum emphasis on the morphing error achievable).

For the remaining analyses, the weighting parameter value of $C = 10^7$ was chosen to ensure that the primary focus of the optimization would be on the morphing error. Table 2.7 shows the three morphing target shapes considered (elliptic, square, and step-type), the optimal design solutions for each target shape, and the corresponding temperature distributions at the initiation of morphing, final stress distributions, and final deformed shapes. All of the optimal design solutions can be seen to have produced recognizable approximations to the target shapes, which is particularly significant considering that each of the three shapes is considerably different from one another and yet the morphing mechanism (i.e., activators and actuators) used to achieve the shapes is identical. However, there was a degradation in the morphing accuracy as the complexity of the target shape change increased, which is not

Table 2.7: Optimized (Opt) design solutions (temperature distribution and final stress distribution) with respect to three different target shapes (ellipse, square and step-type) for Example 2: Morphing Structural Backbone.



necessarily unexpected. This morphing accuracy can be seen quantitatively through the relative difference between the optimized morphing error (S_{opt}) and the morphing error for the starting shape (S_0), which was approximately 90% for the elliptic shape, 40% for the square shape, and 10% for the step-type shape. The target step-type shape was clearly the most challenging to achieve, both intuitively and based on the optimization results, particularly since it was the only shape that required a change from convex to concave. Furthermore, the results would imply that to better achieve a target shape similar to the step-type the starting shape or the morphing mechanisms (i.e., activators and actuators) would need further modification. However, overall, the multiple localized activations and actuations showed the capability to accurately and efficiently achieve a diverse set of shape changes with a fixed set of morphing mechanisms, and the computational approach was particularly well-suited to facilitate the implementation, particularly where intuitive design approaches would be infeasible.

2.7 CONCLUSIONS

A computationally efficient computational mechanics-based strategy to identify the distribution and sequencing of localized activation and actuation for a morphing smart material structure or structural component to optimally obtain a target shape change or set of shape changes was presented. The strategy combines a numerical representation of the behavior of a smart material structure subject to an activation and actuation process with a non-linear optimization algorithm to estimate the optimal activation and actuation parameters that may include minimizing cost functions which address energy consumption, target shape changes, morphing time, and/or damage. In particular, in contrast to the previous study [94], a formulation of the adjoint method was presented to be used within a gradient-based optimization strategy for minimally computationally expensive (i.e., expense equivalent to only two evaluations of initial boundary value problems) computation of the gradient of the optimal design/control objective function(s) with respect to the design/control parameters, and thus, minimally computationally expensive optimization. Two numerical examples

were used to investigate the computational approach in which the synchronization of multiple activators and actuators was optimized with respect to the energy cost and target shape changes in morphing skeletal structural components. The computational optimal design/control approach with the adjoint method was verified with the numerical examples, and some limitations were identified in terms of the local nature of the optimized solutions in comparison to a substantially more computationally expensive non-gradient-based optimization approach. However, in all cases the computational optimal design/control approach with the adjoint method was shown to provide the capability to efficiently identify activation and actuation parameters to achieve energy-efficient morphing capabilities. Moreover, the computational approach was shown to be capable of determining design/control solutions for a diverse set of target shape changes with fixed instrumentation, providing the potential for substantial functionality beyond what could be expected through traditional empirical design strategies.

3.0 A COMPUTATIONAL INVESTIGATION OF THE EFFECTS OF NONLINEAR THERMAL BEHAVIOR ON THE DESIGN OF LOCALLY ACTIVATED THERMALLY RESPONSIVE SMART MATERIAL MORPHING STRUCTURES

3.1 ABSTRACT

An investigation of the effects of nonlinear thermal behavior on the design of locally activated thermally responsive smart material morphing structures is presented. A computational design framework was used for the investigation, which combines a numerical representation of the behavior of a smart material structure subject to an activation and actuation process with a nonlinear optimization algorithm to estimate the optimal activation and actuation parameters that may include minimizing cost functions addressing energy consumption, target shape changes, morphing time, and/or damage. In particular, nonlinear thermal material behavior, as has been observed in some thermally responsive smart materials, but not yet addressed in this context, was included in this computational approach in the numerical representation. Two numerical examples were used to explore and evaluate the effects of this nonlinearity of the thermal behavior. The computational optimal design/control approach was shown to provide the capability to efficiently identify activation and actuation parameters to achieve energy-efficient and accurate morphing capabilities, even when considering the material thermal nonlinearity. More importantly, in all cases, the nonlinearity in the thermal behavior was shown to have a significant influence on the morphing process, and ultimately the design solutions, and should be included in the thermo-mechanical modeling in order to achieve more accurate and better design or control of such morphing systems.

3.2 INTRODUCTION

Overall, there is a broad range of research efforts seeking solutions for the implementation of morphing structure concepts, such as transformable structures [18, 41, 43, 83, 83], deployable structures [2, 24, 46, 52, 79, 104], and morphing aircraft [7, 17, 22, 23, 76, 87, 88, 89, 97, 98, 99, 106], among others. This research includes efforts relating to mechanisms to facilitate morphing as well as the manufacturing processes to build such structures. In particular, a great amount of research presently focuses on the integration of new materials into morphing structure concepts. Of particular interest have been “smart” active materials that have intrinsically controllable material properties, (e.g., materials that can be softened or hardened on command through some input activation), with the present work focused on thermally responsive shape memory polymers (SMP) [26, 118] or similar materials. In a typical thermally responsive SMP cycle, a sample starts in an initial configuration, is stimulated with some controlled thermal activation to reduce the stiffness, the sample is then deformed into a desired new configuration, and when the deformation is complete the stimulus is removed (i.e., the material is cooled) to restore the stiffness and lock the shape.

Previous work has developed a computational approach for the design of smart material morphing structures and preliminarily utilized this approach to investigate the capabilities to design locally activated thermally responsive smart material morphing structures [93, 94, 95]. In this computational approach, a numerical representation (e.g., finite element model) of the morphing structure is first created, noting that this simulation should accurately represent the expected behavior of the device considered in order to achieve accurate design solutions. Moreover, modeling the morphing process for a smart material structure accurately can be a potentially complicated process [20, 51, 56], involving multiple coupled physical processes, nonlinearity, and/or other features that are challenging to model and address numerically. An objective function and corresponding set of constraints are then defined that measure the difference between the numerically approximated response given a set of unknown design variables and the system behavior that is desired. Lastly, a nonlinear optimization algorithm is applied to find the design variables that minimize the objective function. This computational inverse mechanics approach was shown in the previous studies through numerical tests

to provide a generalized and flexible means to facilitate the use of smart material structures to achieve desired morphing processes with controllable localized activation and actuation. However, in these previous proof-of-concept numerical tests (e.g., [94]), for simplicity the behavior of the structures was assumed to be defined by linear transient heat transfer and linear elastic quasi-static solid mechanics, which is clearly not realistic for many foreseeable implementation scenarios. Focusing on one particular aspect for the present work, recent research studies have shown that the changes in the thermal properties of SMP with respect to temperature have significant effect on the predictions of the thermal behaviors in the activation process [16, 80]. Yet, neither the previous studies nor other works relating to computational methods for smart material morphing structures [34, 71, 101], which have been relatively limited in number, have considered this thermal behavior nonlinearity. Overall, neglecting the nonlinearity of the thermal behavior would be expected to be especially significant in the context of designing or controlling locally activated thermally responsive smart material structures, as this could have a substantial impact on the predicted time and energy required to transition the material during the morphing process, both of which are commonly considered critical design components.

To investigate the significance of the nonlinearity in the thermal material properties of a locally activated thermally responsive smart material morphing structure, this work presents a numerical study of the morphing behavior, and more importantly, the design solutions achieved by a computational inverse mechanics procedure applied to such a structure, both with and without inclusion of nonlinear thermal properties. The details for the computational design approach for such smart material morphing structures is presented in Section 3.3. The forward model used to predict the thermally responsive smart material structure behavior and the gradient-based optimization algorithm used within the computational design approach are presented in Sections 3.4 and 3.5, respectively. Then, two design example problems of skeletal structural components are presented in Section 3.6 to evaluate the effects of the nonlinearity of the thermal modeling and to investigate the capabilities of the computational approach, which is followed by the concluding remarks in Section 3.7.

3.3 COMPUTATIONAL DESIGN APPROACH FOR LOCALLY ACTIVATED MORPHING STRUCTURES

Utilizing a standard computational approach, the design/control problem can be cast as a PDE constrained optimization problem. The design/control objectives for the present study were assumed to be minimizing the total energy of the morphing process ($J = J_T + J_W$) and/or achieving a desired shape change by minimizing a morphing error metric (S). The total thermal energy (J_T) required for activation and the total mechanical work (J_W) required for actuation can be determined, respectively, through:

$$J_T = \int_t \int_{\Omega} \rho c(T) [T(\vec{x}, t) - T_0] \delta(t - t_F) d\vec{x} dt \quad (3.1)$$

and

$$J_W = \int_t \int_{\Gamma} \boldsymbol{\sigma}(\vec{x}, t) \cdot \vec{n}(\vec{x}) \cdot \vec{u}(\vec{x}, t) d\vec{x} dt, \quad (3.2)$$

where ρ is the mass density, c is the temperature-dependent specific heat, $\boldsymbol{\sigma}$ is the Cauchy stress tensor, T is the temperature, \vec{u} is the displacement vector, Ω is the spatial domain, Γ is the domain boundary, \vec{n} is the unit outward normal vector on the boundary, and δ is the Dirac delta function. In addition, the morphing error was defined as the difference between a desired displacement field and the displacement field predicted by the forward problem simulation at the completion of the morphing process, as:

$$S = \int_t \int_{\Omega} \sum_{m=1}^M [\vec{u}(\vec{x}, t) - \vec{u}^{target}(\vec{x}, t)]^2 \delta(\vec{x} - \vec{x}_m^*) \delta(t - t_F) d\vec{x} dt, \quad (3.3)$$

where \vec{u} and \vec{u}^{target} are the predicted and desired (i.e., target) displacement fields, respectively, $\{\vec{x}_m^*\}_{m=1}^M$ is the set of M discrete spatial locations where the target displacement is desired to be achieved by the morph, and t_F is the time at the completion of the morphing process.

Although addressing both the energy and morphing error constitutes a multi-objective optimization problem, as is commonly done, for the present work the multi-objective optimization problem was transformed into a single objective problem by simply using a weighted

sum of the two objectives. As such, the final objective function for the design/control optimization utilized herein can be shown as:

$$f(\vec{p}) = J(\vec{p}) + C \cdot S(\vec{p}) \quad (3.4)$$

where \vec{p} is the vector of unknown design parameters to be determined through the optimization (i.e., activation and actuation parameters) and C is the scalar weighting constant (note that the specific value of the weighting constant allows emphasis of the optimization effort to be placed on a specific objective, energy or shape, depending on the relative importance for a particular application). As discussed in the Introduction, this constrained optimization problem was solved herein by using a numerical representation of the morphing system (i.e., forward problem) to predict the value of the design objective function given a set of design parameter values, and then applying a nonlinear optimization strategy to identify the parameters that minimize the objective function while satisfying the required constraints, as detailed in the following.

3.4 FORWARD PREDICTION OF MORPHING STRUCTURE BEHAVIOR

As was done in previous studies, the structures considered here were assumed to be composed entirely of thermally responsive SMP subject only to applied thermal activation and mechanical actuation. At the continuum level the coupled thermo-mechanical behavior of such a structure could be theoretically described by the conservation of mass, linear and angular momentum, and energy. Focusing on the effects of the nonlinearity in the thermal behavior, the behavior of the structures considered was assumed to be defined by nonlinear transient heat transfer coupled with linear elastic quasi-static solid mechanics, and represented by the following initial boundary value problem:

$$\nabla \cdot [k(T)\nabla T(\vec{x}, t)] = \rho c(T) \frac{\partial T(\vec{x}, t)}{\partial t}, \quad \forall \vec{x} \in \Omega, t \in [0, t_F], \quad (3.5)$$

$$\nabla \cdot \boldsymbol{\sigma}(\vec{x}, t) = \vec{0}, \quad \forall \vec{x} \in \Omega, t \in [0, t_F], \quad (3.6)$$

$$T(\vec{x}, 0) = T_0, \quad \forall \vec{x} \in \Omega, \quad t = 0, \quad (3.7)$$

$$T(\vec{x}, t) = T^A(\vec{x}, t), \quad \forall \vec{x} \in \Gamma_T, \quad t \in [0, t_F], \quad (3.8)$$

$$-k(T)\nabla T(\vec{x}, t) \cdot \vec{n}(\vec{x}) = q^A, \quad \forall \vec{x} \in \Gamma_q, \quad t \in [0, t_F], \quad (3.9)$$

$$\vec{u}(\vec{x}, t) = \vec{u}^A(\vec{x}, t), \quad \forall \vec{x} \in \Gamma_U, \quad t \in [0, t_F], \quad (3.10)$$

$$\boldsymbol{\sigma}(\vec{x}, t) \cdot \vec{n}(\vec{x}) = \vec{\tau}^A(\vec{x}, t), \quad \forall \vec{x} \in \Gamma_{\vec{\tau}}, \quad t \in [0, t_F], \quad (3.11)$$

$$\boldsymbol{\sigma}(\vec{x}, t) = \mathbf{C}^{IV}(E(T), \nu) : \boldsymbol{\epsilon}(\vec{x}, t), \quad \forall \vec{x} \in \Omega, \quad t \in [0, t_F], \quad (3.12)$$

$$\boldsymbol{\epsilon}(\vec{x}, t) = \frac{1}{2}[\nabla \vec{u}(\vec{x}, t) + \nabla \vec{u}(\vec{x}, t)^T], \quad \forall \vec{x} \in \Omega, \quad t \in [0, t_F], \quad (3.13)$$

where k is the temperature-dependent thermal conductivity, ρ is the mass density, c is the temperature-dependent specific heat, $\boldsymbol{\sigma}$ is the Cauchy stress tensor, $\boldsymbol{\epsilon}$ is the small strain tensor, \mathbf{C}^{IV} is the fourth order elastic stiffness tensor, E is the Young's modulus, ν is the Poisson's ratio, \vec{u} is the displacement vector, Ω is the spatial domain, Γ is the domain boundary, \vec{n} is the unit outward normal vector on the boundary. Γ_T is the portion of the domain boundary where the temperature is specified, Γ_q is the portion of the domain boundary where the heat flux is specified, Γ_U is the portion of the domain boundary where the displacement is specified, and $\Gamma_{\vec{\tau}}$ is the portion of the domain boundary where the traction is specified.

The specific material parameters used for the examples were chosen based on those published for the commercially available thermally responsive SMP VeriflexE [16, 44, 78]. Figure 3.1 shows the relationship between the elastic modulus and temperature, with the modulus varying between $3260MPa$ in the glassy state to $1.69MPa$ in the rubbery state when heated above the glass transition temperature ($T_g = 104^\circ C$ or $377.15K$). Figure 3.2

Table 3.1: The assumed material parameters for the numerical study.

Material Parameter	Value
Poisson's ratio	0.45
Density	$920kg/(m^3)$
Convective heat transfer coefficient	$25W/(m^2 \cdot K)$

shows the relationship between the thermal conductivity and temperature, with the conductivity varying between $0.206 W/m \cdot K$ in the glassy state to $0.234 W/m \cdot K$ in the rubbery state when heated above the glass transition temperature. Figure 3.3 shows the relationship between the specific heat and temperature, with the specific heat varying between $1670 J/Kg \cdot K$ in the glassy state to $2650 J/Kg \cdot K$ in the rubbery state when heated above the glass transition temperature. The remaining mechanical and thermal material parameters are shown in Table 3.1. For all forward problem analyses in this study, the coupled thermo-mechanical behavior described by Eqns. 3.5 - 3.13 was simulated using the standard Galerkin finite element method [90].

3.5 GRADIENT-BASED OPTIMIZATION USING ADJOINT METHOD

While a genetic algorithm (as used in [94]) was considered in past studies due to its global search capabilities, the present work solely utilized gradient-based optimization to focus on computational efficiency of the design/control solution procedure, particularly relying on the adjoint approach to expedite gradient calculations, for the minimization of Eqn. 3.4. A quasi-Newton gradient-based algorithm, the BFGS interior point algorithm [3, 61, 86], was chosen for the gradient based optimization, and the details of the adjoint approach to calculate the gradient of the objective function (f) with respect to the design parameters (\vec{p}) to drive this gradient-based optimization process for the previously defined forward problem

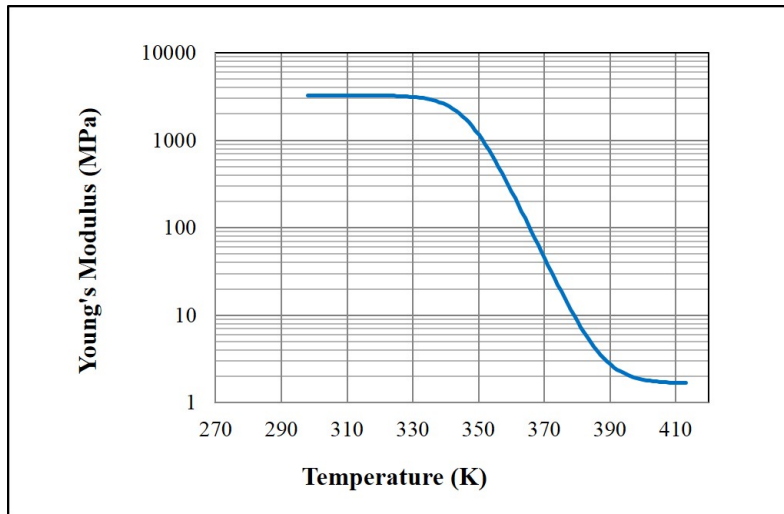


Figure 3.1: The assumed relationship between Young's modulus and temperature for the numerical study.

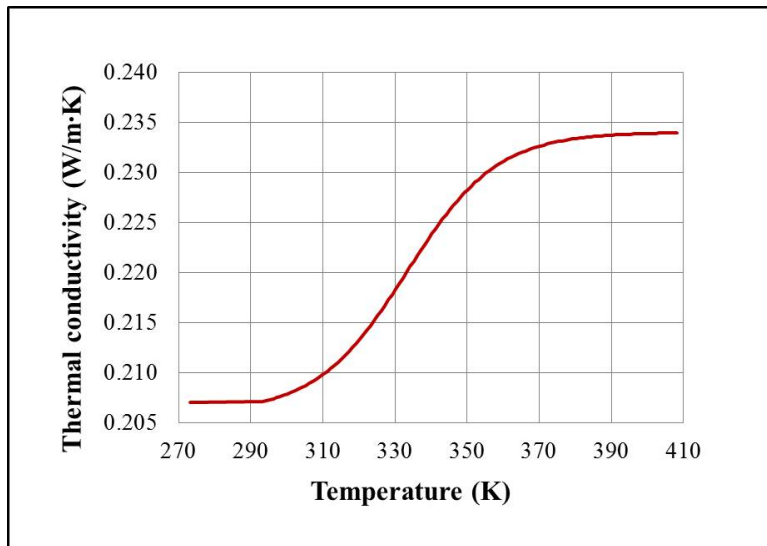


Figure 3.2: The assumed relationship between thermal conductivity and temperature for the numerical study.

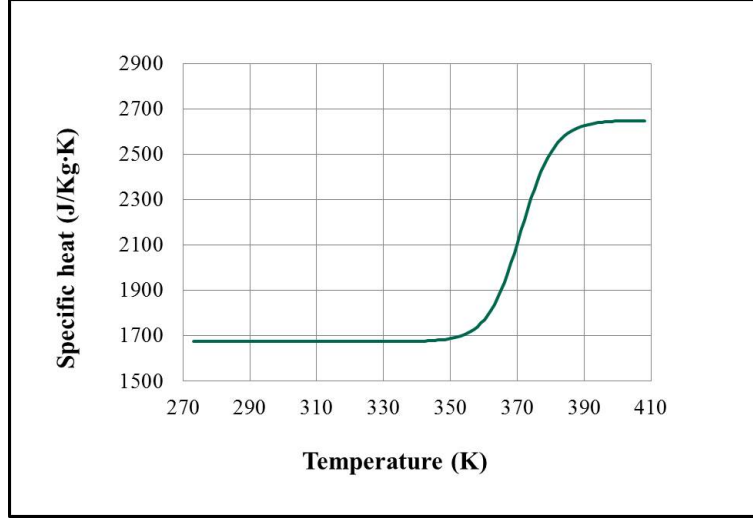


Figure 3.3: The assumed relationship between specific heat and temperature for the numerical study.

are presented in the following. In general, the algorithm for the calculation of the gradient of the objective function with respect to the design parameters using the adjoint method can be summarized as follows:

- (1) Solve the forward initial boundary value problem (Eqns. 3.5 - 3.13) to obtain the displacement field \vec{u} and the temperature field T .
- (2) Solve the adjoint initial boundary value problem (Eqns. 3.14 - 3.20) to obtain the Lagrange multipliers λ and $\vec{\varphi}$.
- (3) Substitute \vec{u} , T , λ and $\vec{\varphi}$ into Eqn. 3.21 to compute the gradient of the objective function.

The overall key to the adjoint method is the formulation of an adjoint (initial boundary value) problem in terms of a set of Lagrange multipliers that is derived from the objective functional and the associated forward problem[6, 25, 32, 45, 114].

For the objective function and forward problem presented, the following adjoint problem for the Lagrange multipliers λ and $\vec{\varphi}$ can be derived:

$$k(T) \nabla^2 \lambda + \rho c(T) \frac{\partial \lambda}{\partial t} + \rho \left[\frac{\partial c}{\partial T} (T - T_0) + c(T) \right] \delta(t - t_F) - \frac{1}{E} \frac{\partial E}{\partial T} (\nabla \vec{\varphi}) : \boldsymbol{\sigma}_{\vec{u}} = 0, \quad (3.14)$$

$$\nabla \cdot \boldsymbol{\sigma}_{\vec{\varphi}}(\vec{x}, t) + C \sum_{m=1}^M 2[\vec{u} - \vec{u}^{target}] \delta(\vec{x} - \vec{x}_m^*) \delta(t - t_F) = \vec{0}, \quad \forall \vec{x} \in \Omega, t \in [0, t_F], \quad (3.15)$$

$$\lambda(\vec{x}, t_F) = 0, \quad \forall \vec{x} \in \Omega, t = t_F, \quad (3.16)$$

$$\lambda(\vec{x}, t) = 0, \quad \forall \vec{x} \in \Gamma_T, t \in [0, t_F], \quad (3.17)$$

$$-k(T) \nabla \lambda(\vec{x}, t) \cdot \vec{n}(\vec{x}) = 0, \quad \forall \vec{x} \in \Gamma_q, t \in [0, t_F], \quad (3.18)$$

$$\vec{\varphi}(\vec{x}, t) = -\vec{u}^A(\vec{x}, t), \quad \forall \vec{x} \in \Gamma_U, t \in [0, t_F], \quad (3.19)$$

$$\boldsymbol{\sigma}_{\vec{\varphi}}(\vec{x}, t) \cdot \vec{n}(\vec{x}) - \vec{\tau}^A \delta(t - t_F) + \frac{\partial \vec{\tau}^A}{\partial t} = \vec{0}, \quad \forall \vec{x} \in \Gamma_{\vec{\tau}}, t \in [0, t_F]. \quad (3.20)$$

After solving the above adjoint problem for the Lagrange multipliers, the gradient of the Lagrangian, and by extension, the gradient of the objective function can be calculated as:

$$\begin{aligned} \frac{dL}{dp_j} &= \int_t \int_{\Gamma_T} (-k \nabla \lambda \cdot \vec{n}) \frac{\partial T^A}{\partial p_j} d\vec{x} dt + \int_t \int_{\Gamma_U} (-\boldsymbol{\sigma}_{\vec{\varphi}} \cdot \vec{n} \cdot \frac{\partial \vec{u}^A}{\partial p_j} + \boldsymbol{\sigma}_{\vec{u}} \cdot \vec{n} \cdot \frac{\partial \vec{u}^A}{\partial p_j}) d\vec{x} dt \\ &\quad - \int_t \int_{\Gamma_q} (\lambda \frac{\partial q^A}{\partial p_j}) d\vec{x} dt + \int_t \int_{\Gamma_{\vec{\tau}}} (\vec{\varphi} + \vec{u}^A) \frac{\partial \vec{\tau}^A}{\partial p_j} d\vec{x} dt, \end{aligned} \quad (3.21)$$

where

$$\boldsymbol{\sigma}_{\vec{u}} = \frac{E}{2(1+\nu)}[\nabla\vec{u} + \nabla(\vec{u})^T] + \frac{E}{(1+\nu)(1-2\nu)}(\nabla \cdot \vec{u})\mathbf{I} \quad (3.22)$$

and

$$\boldsymbol{\sigma}_{\vec{\varphi}} = \frac{E}{2(1+\nu)}[\nabla\vec{\varphi} + \nabla(\vec{\varphi})^T] + \frac{E}{(1+\nu)(1-2\nu)}(\nabla \cdot \vec{\varphi})\mathbf{I}, \quad (3.23)$$

and \mathbf{I} is the identity tensor. Similar to the forward initial boundary value problem, in the present work the adjoint problem was solved using the traditional Galerkin finite element method.

3.6 NUMERICAL INVESTIGATION

To investigate the effects of nonlinear thermal behavior on the design of locally activated thermally responsive smart material morphing structures, a numerical investigation was performed with two example morphing structure concepts. First, a relatively geometrically simple example of a morphing structural backbone was tested. Then, a more realistic example of a morphing airfoil structure with substantially increased complexity of design parameters compared to the first example was considered.

3.6.1 Example 1: Morphing Structural Backbone

Similar to the examples considered in the previous investigations in Section 2.6, the concept of a morphing structural backbone considered here implies a structural element that is directly connected to the exposed surface of the structure, and therefore, the overall shape of the backbone, not just the positioning of the endpoints, affects the function of the structure. For example, this type of morphing component could be installed in the edge of an aerodynamic structure, for which it may be desirable to use the component to prescribe both the size as well as the shape of all or some part of the structure's surface. A schematic of the structural backbone considered for this first example is shown in Figure 3.4. The structure was taken to be a homogeneous half-circular prism with a 150mm outer radius, and the structure was analyzed using the plane strain assumption.

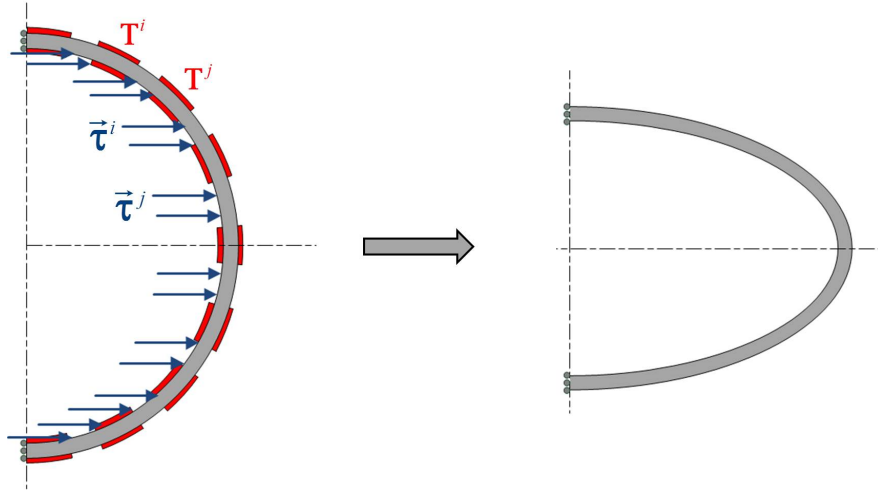


Figure 3.4: Schematic of Example 1: Morphing Structural Backbone.

For the morphing procedure, the total time to perform the structural morphing, t_F , was simply the summation of the purely heating time prior to actuation, t_D , and the actuation time, t_M . A total of nine pairs of approximately 45mm long heating pads (i.e., 18 total heating pads) and eight approximately 15mm long actuation regions, all equally spaced along the surface of the structure. Additionally, the operation of the structure and the design/control objectives were assumed to be symmetric with respect to the horizontal axis. Thus, only the top half to the structure needed to be analyzed and the morphing process of the structure was defined by 10 independent heating pads and four actuators. The entire structure was assumed to be initially at room temperature (293K), and the 10 heating pads along the outer and inner surface of the structure were heated independently (i.e., prescribing a different t_T^i for each heating pad). Temperature was assumed to be applied uniformly throughout the length of each heating pad and to increase linearly in time on that region starting from room temperature at a fixed rate of 1.15K/s for a controllable “warm-up” duration (in effect defining the maximum applied temperature), t_T , and then held constant until morphing was completed. The portion of the boundary not being heated was assumed to be insulated. The two ends of the structure were assumed to be constrained

Table 3.2: Applied traction boundary conditions for Example 1: Morphing Structural Backbone.

	$0 \leq t \leq t_D$	$t_D \leq t \leq t_F$
	$\tau_1^A(\vec{x}, t) = 0$	$\tau_1^A(\vec{x}, t) = \frac{\tau_1^i}{t_M} \cdot (t - t_D)$
Actuated Boundary $\{\Gamma_{\vec{\tau}}^i\}_{i=1}^4$	$\tau_2^A(\vec{x}, t) = 0$	$\tau_2^A(\vec{x}, t) = 0$

in the horizontal direction and the amplitude of the horizontal tractions (τ_1^i) over each actuation region was controllable and assumed to increase linearly in time to deform the structure, while the remaining boundaries were taken to be traction free. The actuator traction boundary conditions that were applied uniformly over the length of each actuation region are described in Table 3.2.

For this example, neither the time to complete the deformation nor the heating time prior to actuation had a significant effect on the design objectives, and thus were fixed at values of $t_M = 10s$ and $t_D = 590s$. Therefore, the chosen design variables to be determined in this example were the warm-up time for each heating pad and the maximum amplitude of the actuation force, such that $\vec{p} = [t_T^1, t_T^2, \dots, t_T^{10}, \tau_1^1, \tau_1^2, \tau_1^3, \tau_1^4]$. Table 3.3 shows a summary of the constrained optimization problem constructed for this morphing structural backbone example. The gradient-based algorithm was applied with 10 randomly selected initial parameter vector values and selecting the best result from these 10 outcomes as the final solution estimate, and using a relative change in the objective function value of 0.005% as the stopping criteria for each trial.

Firstly, to obtain an initial understanding of the influence of the nonlinearity in the thermal modeling on the morphing process, a comparison between the heating process of the morphing structural backbone system with linear (i.e., constant) thermal properties and nonlinear thermal properties (i.e., the temperature-dependent thermal properties defined previously) was carried out. Table 3.4 shows the linear properties utilized. To make the comparison, the same amount of thermal energy (i.e., heating flux input on the heating

Table 3.3: Summary of the optimization objective and constraints for Example 1: Morphing Structural Backbone.

Objective Function	$f = J + C \cdot S$
Design Parameters	$0 < t_T^i \leq 100s, (i = 1, 2, 3 \dots 10.)$
and Constraints	$0 < \tau_1^i \leq 0.1MPa, (i = 1, 2, 3, 4.)$
	$\ \sigma^{von} \ _{L^\infty(\Omega)} \leq 11.5MPa$

pads) was given to the same morphing systems, and the heating processes with the various thermal properties were compared. Then, to explore the influence of the thermal nonlinearity on the design process, a set of shape targets with varying levels of complexity was considered (e.g., square and step-type target shapes). The optimization process was performed for the morphing structural backbone system with both the linear and the nonlinear thermal behaviors used, in turn, and the optimization results were compared. For all design trials, the weighting parameter value of $C = 10^7$ was chosen to ensure that the primary focus of the optimization would be on the morphing error.

3.6.1.1 Results and Discussion: Figure 3.5 shows the temperature distribution for the morphing backbone with linear thermal properties and nonlinear thermal properties, both using the same amount of thermal input energy. As can be seen, the temperature within the

Table 3.4: Assumed material parameters for linear thermal behavior.

Material Parameter	Value
Thermal conductivity	$0.206W/(m \cdot K)$
Specific heat	$1670J/(kg \cdot K)$

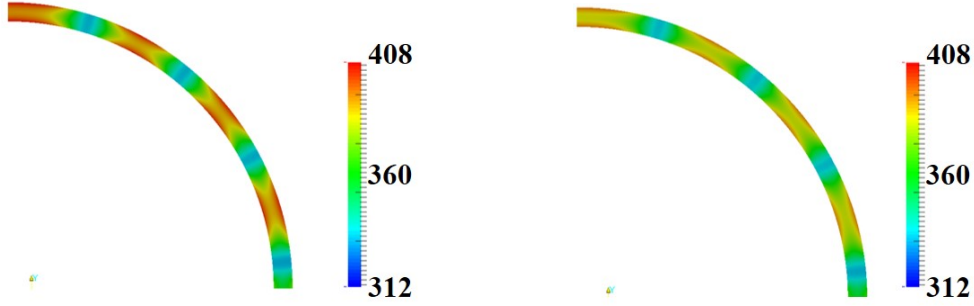
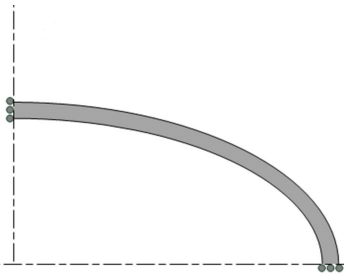
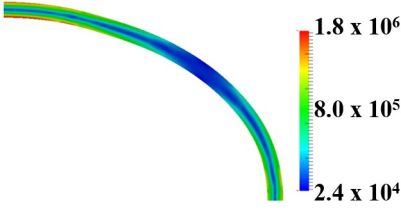
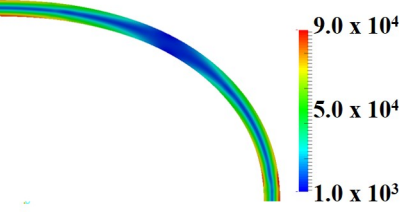
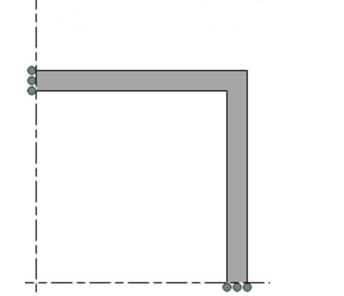
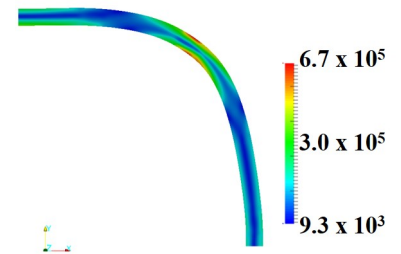
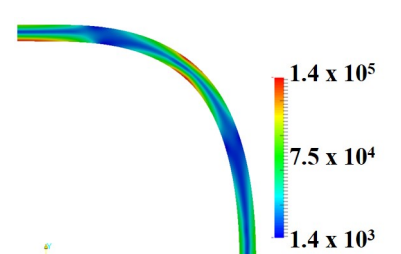
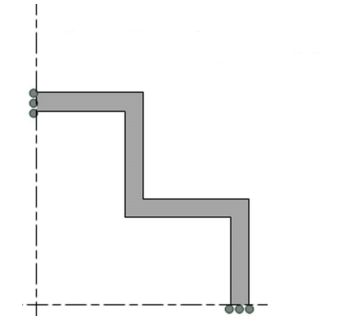
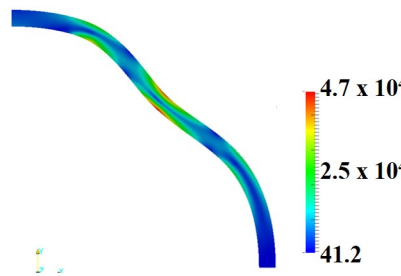
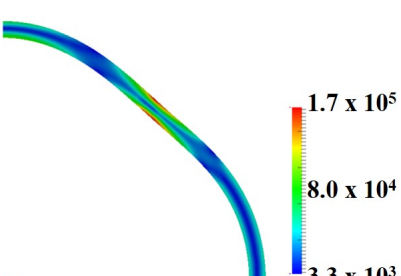


Figure 3.5: Temperature distribution (K) for the morphing system with (a) linear thermal properties and (b) nonlinear thermal properties for Example 1: Morphing Structural Backbone.

backbone increased considerably faster for the case with linear thermal properties in comparison to the case with nonlinear thermal properties. This heating difference is explained by the fact that although the nonlinear behavior had a higher thermal conductivity in the example conditions, the specific heat was higher as well, which resulted in a lower overall thermal diffusivity within the conditions considered in this example. This significant difference in the temperature distribution between the linear and nonlinear behaviors highlights the importance of the thermal behavior modeled. In particular, using linear thermal properties when the behavior is actually nonlinear could lead to substantial errors in the transient temperature distribution predictions as well as the prediction of the thermal energy required in the morphing system.

Table 3.5 shows three morphing target shapes considered (elliptic, square, and step-type) and the corresponding optimal design solutions estimated for both the linear and nonlinear thermal property scenarios. As can be seen, the optimal design solutions for both the linear and nonlinear thermal property scenarios produced recognizable approximations to the target shapes. However, there was a significant difference in the morphing errors of the optimized design solutions between the linear and nonlinear cases. Therefore, these example cases show how using linear thermal properties where nonlinear exist would lead to a relatively large inaccuracy in the parameters predicted by the design optimization process,

Table 3.5: Optimized design solutions (final stress distribution) with respect to three different target shapes (ellipse, square and step-type) for the linear thermal property and the nonlinear thermal property scenarios for Example 1: Morphing Structural Backbone.

Target Shape	Stress Distribution (Pa) (Linear Thermal Modeling)	Stress Distribution (Pa) (Nonlinear Thermal Modeling)
		
		
		

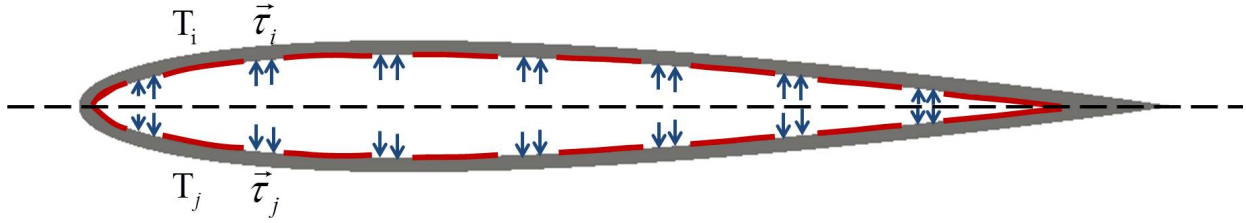


Figure 3.6: Schematic of the Morphing Airfoil Structure Design Concept for Example 2.

and thus, the actual shape that would be achieved with parameters determined from this design process (if assumed linear) applied to the actual structure (if actually nonlinear). Moreover, for the specific example case shown here, the optimization with linear behavior noticeably overestimates the ability of the given morphing structure to achieve the desired shapes (particularly the step-type shape) subject to the constraints enforced on the system.

3.6.2 Example 2: Morphing Airfoil Structures

The second numerical example focused on a more realistic case study of a morphing airfoil structure, shown schematically in Figure 3.6. The geometry of the example was based on a standard NACA-0012 cross section [1]. The structure was taken to be a homogeneous and the structure was again analyzed using the plane strain assumption.

The morphing procedure applied followed a similar sequencing pattern as the first example. However, to provide greater degrees of freedom for the design/control of the morphing system, several more heating pads and actuators were employed in this case compared to the first example, with a total of 16 approximately 95mm long heating pads and 14 approximately 30mm long actuation regions, all equally spaced along the inner surface of the structure. The entire structure was assumed to be initially at room temperature (293K), and the 16 heating pads along the inner surface of the structure were heated independently (i.e., prescribing a different t_T^i for each heating pad) following the same heating pattern as was used in the first example problem. The two ends of the structure were assumed to be

Table 3.6: Applied traction boundary conditions for Example 2: Morphing Airfoil Structure.

	$0 \leq t \leq t_D$	$t_D \leq t \leq t_F$
Actuated Boundary $\{\Gamma_{\vec{\tau}}^i\}_{i=1}^{14}$	$\tau_1^A(\vec{x}, t) = 0$	$\tau_1^A(\vec{x}, t) = 0$
	$\tau_2^A(\vec{x}, t) = 0$	$\tau_2^A(\vec{x}, t) = \frac{\tau_2^i}{t_M} \cdot (t - t_D)$

fully constrained and the amplitude of the vertical tractions (τ_1^i) over each actuation region was controllable and assumed to increase linearly in time to deform the structure, while the remaining boundaries were taken to be traction free. The actuator traction boundary conditions that were applied uniformly over the length of each actuation region are described in Table 3.6.

Similarly to the previous example, neither the time to complete the deformation nor the heating time prior to actuation had a significant effect on the design objectives, and were again fixed at values of $t_M = 10s$ and $t_D = 1190s$. Therefore, the chosen design variables to be determined in this example were the warm-up time for each heating pad and the maximum amplitude of the actuation force, such that $\vec{p} = [t_T^1, t_T^2, \dots, t_T^{16}, \tau_2^1, \tau_2^2, \tau_2^3, \tau_2^{14}]$. The target shape considered in the design problem for this example was to achieve 2% max camber at position 40%, as shown in Figure 3.7. Table 3.7 shows a summary of the constrained optimization problem constructed for this morphing airfoil structure example. The optimization process



Figure 3.7: Target Airfoil Shape with 2% Max Camber at Position 40%.

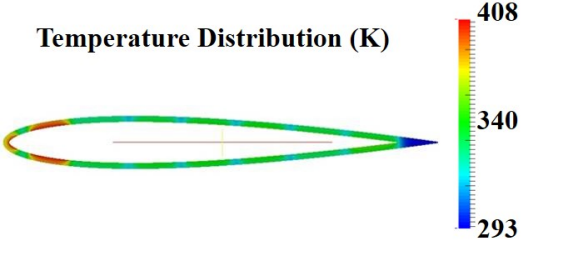
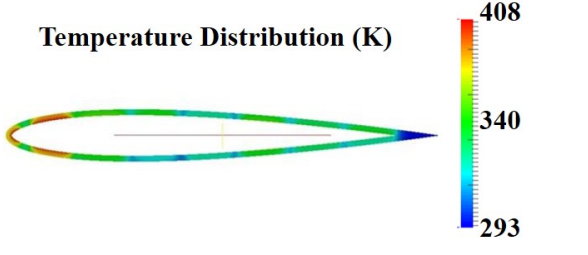
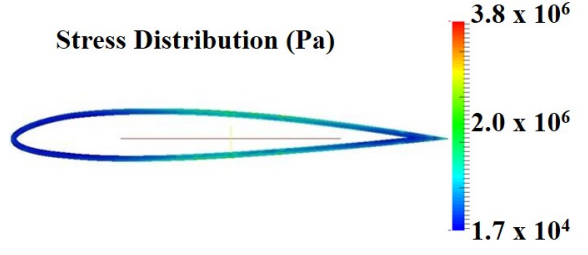
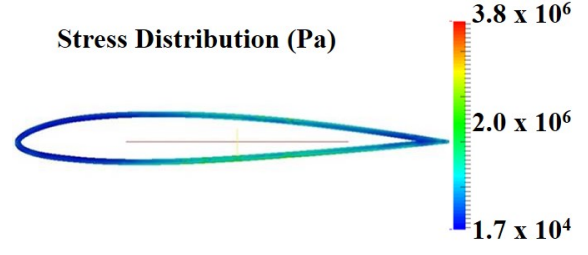
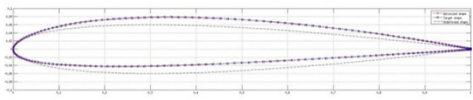
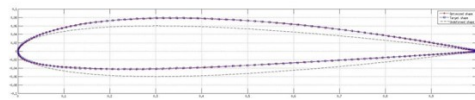
Table 3.7: Summary of the optimization objective and constraints for Example 2: Morphing Airfoil Structure.

Objective Function	$f = J + C \cdot S$
Design Parameters	$0 < t_T^i \leq 100s, (i = 1, 2, 3 \dots 16.)$
and Constraints	$0 < \tau_1^i \leq 0.1MPa, (i = 1, 2, 3 \dots 14.)$
	$\ \sigma^{von} \ _{L_\infty(\Omega)} \leq 11.5MPa$

was performed for the airfoil with the same linear and the nonlinear thermal behaviors from the first example used, in turn, and the optimization results were compared. The gradient-based optimization algorithm with the adjoint method was again applied with 10 randomly selected initial parameter vector values and selecting the best result from these 10 outcomes as the final solution estimate, but the stopping criteria was changed for this example to be a morphing error value of 5×10^{-6} . Therefore, approximately the same final morphing error could be achieved for all trials with both material behaviors, and the energy required to perform the morphing process (i.e., efficiency) could instead be compared between test cases.

3.6.2.1 Results and Discussion: Table 3.8 shows the optimal design solutions (temperature distribution and final stress distribution) estimated for both the linear and nonlinear thermal property scenarios. As can be seen, the optimal design solutions for both the linear and nonlinear thermal behaviors produced almost identical approximations to the target shape, which were nearly exact matches. However, there was a significant difference in the thermal energy required to obtain the same morphing error ($S = 5 \times 10^{-6}$) between the two material behaviors, with $J = 523MJ$ of energy estimated to be required with the linear thermal behavior and $J = 682MJ$ of energy estimated to be required with the nonlinear thermal behavior. In other words, for this example case, the analysis incorporating nonlinear

Table 3.8: Optimized design solutions (temperature distribution and final stress distribution) for the linear thermal property and the nonlinear thermal property scenarios for Example 2: Morphing Airfoil Structure.

Linear Thermal Modeling ($J = 523MJ, S = 5 \times 10^{-4}$)	Nonlinear Thermal Modeling ($J = 682MJ, S = 5 \times 10^{-4}$)
<p>Temperature Distribution (K)</p> 	<p>Temperature Distribution (K)</p> 
<p>Stress Distribution (Pa)</p> 	<p>Stress Distribution (Pa)</p> 
<p>Shape Comparison</p> 	<p>Shape Comparison</p> 

thermal behavior predicted an approximately 23% increase in the required thermal energy in comparison to the prediction with linear thermal behavior. This is clearly a substantial amount of required energy that would be underestimated if designing the system assuming linear thermal behavior where nonlinear actually existed. Such an underestimation could potentially even lead to a morphing system being deployed without a sufficient power supply to perform the desired morphing behavior, or worse.

3.7 CONCLUSIONS

The effects of nonlinear thermal behavior on the design of locally activated thermally response smart material morphing structures were investigated using numerical case studies and a computational design framework. The computational framework combined a numerical representation of the behavior of a smart material structure subject to an activation and actuation process with a nonlinear optimization algorithm to estimate the optimal activation and actuation parameters that would potentially address cost functions including energy consumption, target shape changes, morphing time, and/or damage. In particular, in contrast to previous studies, nonlinear thermal material behavior was included in this computational design approach to investigate the effects of the thermal nonlinearity, which is typically ignored with thermal behavior assumed to be linear, on the design process. Two numerical examples were used to explore and evaluate the effects of the nonlinearity of the thermal behavior, in which the synchronization of multiple activators and actuators was optimized with respect to the energy cost and target shape changes in morphing structural components. In all cases, the nonlinearity in the thermal behavior was shown to have a significant influence on the morphing process, and should be included in the thermo-mechanical modeling in many scenarios in order to achieve design or control parameters that will produce an accurate and functional morphing system.

4.0 CURRENT CAPABILITIES AND FUTURE DIRECTIONS

A computational strategy for computationally efficient estimation of the parameters relating to the distribution and sequencing of activation and actuation for a morphing smart material structure or structural component to efficiently and effectively achieve a desired morphing function has been developed and evaluated. This strategy combines a numerical representation of the morphing process with an optimization algorithm to estimate the activation and actuation parameters that best address cost functions and constraints relating to energy consumption, target shape change(s), morphing time, and/or damage prevention. In particular, the strategy was investigated in the context of morphing structures or structural components composed of thermally responsive smart materials, and with specific properties based on thermally responsive shape memory polymers. In all cases considered to this point, the morphing structural response for the numerical study was assumed to be sufficiently represented by transient linear or nonlinear heat transfer and quasi-static linear elastic solid mechanics.

For the optimization part of the computational framework, both non-gradient based optimization methods (i.e., GA) and gradient-based optimization methods (i.e., adjoint method) were tested. The gradient-based optimization algorithm with the adjoint method was shown to provide a more efficient optimization process comparing to the non-gradient based optimization algorithm. For the forward modeling of the smart material morphing structure, both linear and nonlinear thermal behaviors were tested. The nonlinearity in the thermal behavior was shown to have a significant influence on the morphing process. The computational optimal design/control approach was verified with several numerical examples. In all cases the computational optimal design/control approach with the adjoint method was shown to provide the capability to efficiently identify activation and actuation parameters to

achieve energy-efficient morphing capabilities. Moreover, the computational approach was shown to be capable of determining design/control solutions for a diverse set of target shape changes with fixed instrumentation, providing the potential for substantial functionality beyond what could be expected through traditional empirical design strategies.

In general, certain extensions need to be made in order for the framework to be applicable to realistic scenarios. Specifically, the computational framework should ultimately be upgraded to include both geometric and material nonlinearity (a significantly more realistic condition considering the large strains and deformations that would be expected in a smart material morphing structure). For example, the effect of finite strain, material phase transition, and two-way (i.e., full) coupling should be included in the future thermo-mechanical modeling. In addition, more complex morphed structure geometries and multiple morphing targets should be explored. Moreover, to improve the efficiency of the computational framework while maintaining the accuracy of the inverse solution process, other optimization methods, cost functions and constraint forms can be explored, and various types of reduced order modeling could be considered to further reduce the computational cost without sacrificing accuracy.

BIBLIOGRAPHY

- [1] Naca-0012 <https://airfoiltools.com/airfoil/>.
- [2] Brown M A. A deployable mast for solar sails in the range of 100-1000 m. *Advances in Space Research*, 48(11):1747–1753, 2011.
- [3] Forsgren A, Gill P E, and Wright M H. Interior methods for nonlinear optimization. *SIAM review*, 44(4):525–597, 2002.
- [4] Lendlein A, Jiang H, Junger O, and Langer R. Light-induced shape-memory polymers. *Nature*, 434:879–882, 2005.
- [5] Lendlein A and Langer R. Biodegradable, elastic shape-memory polymers for potential biomedical applications. *Science*, 296:1673–1676, 2002.
- [6] Oberai A A, Gokhale N H, and Feijoo G R. Solution of inverse problems in elasticity imaging using the adjoint method. *Inverse Problems*, 19:297313, 2003.
- [7] Sofla A, Meguid S, Tan K, and Yeo W. Shape morphing of aircraft wing: status and challenges. *Materials and Design*, 31(3):1284–1292, 2010.
- [8] Suzuki A and Tanaka T. Phase transition in polymer gels induced by visible light. *Nature*, 346:345–347, 1990.
- [9] Yousefi-Koma A and Zimicik D G. Applications of smart structures to aircraft for performance enhancement. *Canadian Aeronautics and Space Journal*, 49:163–172, 2003.
- [10] Lattime S B and Steinetz B M. Turbine engine clearance control systems: current practices and future directions. Technical report, NASA, 2002.
- [11] Lu H B, Huang W M, and Yao Y T. Review of chemo-responsive shape change/memory polymers. *Pigment & Resin Technology*, 42(4):237–246, 2013.
- [12] Lu H B and Du S Y. A phenomenological thermodynamic model for the chemo-responsive shape memory effect in polymers based on flory–huggins solution theory. *Polymer Chemistry*, 5(4):1155–1162, 2014.

- [13] Lv H B, Liu Y J, Zhang D X, Leng J S, and Du S Y. Solution-responsive shape-memory polymer driven by forming hydrogen bonding. *Advanced Materials Research*, 47–50:258–261, 2008.
- [14] Lv H B, Leng J S, Liu Y J, and Du S Y. Shape-memory polymer in response to solution. *Advanced Engineering Materials*, 10:592–595, 2008.
- [15] R. Beblo, K. Gross, and L. W. Weiland. Mechanical and curing properties of a styrene-based shape memory polymer. *Journal of Intelligent Material Systems and Structures*, 21:677– 683, 2010.
- [16] Richard Beblo, James Joo, Brian Smyers, and Gregory Reich. Thermal properties of magnetite nanoparticle and carbon fiber doped epoxy shape memory polymer. In *ASME 2011 Conference on Smart Materials, Adaptive Structures and Intelligent Systems*, pages 307–314. American Society of Mechanical Engineers, 2011.
- [17] P. Bourdin, A. Gatto, and M. Friswell. Performing co-ordinated turns with articulated wing-tips as multi-axis control effectors. *Aeronautical Journal*, 114(1151):35, 2010.
- [18] T. Buhl, F. V. Jensen, and S. Pellegrino. Shape optimization of cover plates for retractable roof structures. *Computers and Structures*, 82(15):1227–1236, 2004.
- [19] Chen Y C and Lagoudas D C. A constitutive theory for shape memory polymers. part i: large deformations. *Journal of the Mechanics and Physics of Solids*, 56:1752–1765, 2008.
- [20] Chen Y C and Lagoudas D C. A constitutive theory for shape memory polymers. part i: Large deformations. *Journal of the Mechanics and Physics of Solids*, 56(5):1752–1765, 2008.
- [21] Wang C C, Huang W M, Ding Z, Zhao Y, and Purnawali H. Cooling-/water-responsive shape memory hybrids. *Composites Science and Technology*, 72:1178–1182, 2012.
- [22] L. Campanile. Modal synthesis of flexible mechanisms for airfoil shape control. *Journal of Intelligent Material Systems and Structures*, 19(7):779–789, 2008.
- [23] Baker D and Friswell M. Determinate structures for wing camber control. *Smart Materials and Structures*, 18(3):035014, 2009.
- [24] Z. Q. Deng, Y. Zhang, H. L. Huang, and B. Li. Parametric optimization for a tapered deployable mast in an integrated design environment. *Advanced Materials Research*, 346:426–432, 2012.
- [25] O. Dorn, H. Bertete-Aguirre, J. G. Berryman, and G. C. Papanicolaou. A nonlinear inversion method for 3d electromagnetic imaging using adjoint fields. *Inverse Problems*, 15:152358, 1999.

- [26] R. B. Dupaix and M. C. Boyce. Constitutive modeling of the finite strain behavior of amorphous polymers in and above the glass transition. *Mechanics of Materials*, 39:39–52, 2007.
- [27] Bridges J E, Wernet M, and Brown C. Control of jet noise through mixing enhancement. Technical report, NASA, 2003.
- [28] Goldberg D E. *Genetic algorithms in search, optimization, and machine learning*. Addison-wesley Reading Menlo Park, 1989.
- [29] Havens E, Snyder E A, and Tong T H. Light-activated shape memory polymers and associated applications. *Smart Structures and Materials 2005: Industrial and Commercial Applications of Smart Structures Technologies.*, 5762:48–55, 2005.
- [30] Wornyo E, May G S, and Gall K. Modeling and optimization of the deposition of shape memory polymers for information storage applications. *Semiconductor Manufacturing, IEEE Transactions*, 22:409–416, 2009.
- [31] Calkins F, Bulter G, and Mabe J. Variable geometry chevrons for jet noise reduction. In *Proc. of the 27th Annual AIAA Aeroacoustics Conf.*, pages 8–10, 2006.
- [32] G. R. Feijoo, M. Malhotra, A.A. Oberai, and P. M. Pinsky. Shape sensitivity calculations for exterior acoustics problems. *Engineering Computations*, 18:376 – 393, 2001.
- [33] Dumont G and Kuhl C. Finite element simulation for design optimization of shape memory alloy spring actuators. *Engineering Computations*, 22:835–848, 2005.
- [34] Dumont G and Kuhl C. Finite element simulation for design optimization of shape memory alloy spring actuators. *Engineering Computations*, 22:835–848, 2005.
- [35] Wei Z G, Sandstrom R, and Miyazaki S. Review shape-memory materials and hybrid composites for smart systems part i shape-memory materials. *Journal of Materials Science*, 33:3743–3762, 1998.
- [36] D. E. Goldberg. *Genetic algorithms in search, optimization, and machine learning*. Addison-Wesley Professional, 1989.
- [37] Byrd R H, Gilbert J C, and Nocedal J. *A trust region method based on interior point techniques for nonlinear programming*. Mathematical programming. Springer, 2000.
- [38] Byrd R H, Hribar M E, and Nocedal J. An interior point algorithm for large-scale nonlinear programming. *Siam Journal on Optimization*, 9:877–900, 1999.
- [39] Finkelmann H, Nishikawa E, Pereira G, and Warner M. A new opto-mechanical effect in solids. *Physical Review Letters*, 87, 2001.

- [40] Lin J K H, Knoll C F, and Willey C E. Shape memory rigidizable inflatable (ri) structures for large space systems applications. In *Proc. of 47th AIAA/ASME/ASCE/AHS/ASC Structures, Structural Dynamics, and Materials Conf.*, 2006.
- [41] F. Haldi and D. Robinson. Adaptive actions on shading devices in response to local visual stimuli. *Journal of Building Performance Simulation*, 3(2):135–153, 2010.
- [42] S. Hayashi, Y. Tasaka, N. Hayashi, and Y. Akita. Development of smart polymer materials and its various applications. *Review Literature And Arts Of The Americas*, 41:1–3, 2004.
- [43] C. Hoberman and M. Davis. Panel assemblies for variable shading and ventilation, 2009. US Patent No 7,584,777.
- [44] CRG industries. <http://www.crgpr.com/technology/materialsportfolio/verix.shtml>.
- [45] A. Iollo, M. Ferlauto, and L. Zannetti. An aerodynamic optimization method based on the inverse problem adjoint equations. *Journal of Computational Physics*, 173:87–115, 2001.
- [46] Costantine J, Tawk Y, Christodoulou C G, Banik J, and Lane S. Cubesat deployable antenna using bistable composite tape-springs. *Antennas and Wireless Propagation Letters, IEEE*, 11:285–288, 2012.
- [47] Hartl D J, Lagoudas D C, and Calkins F T. Advanced methods for the analysis, design, and optimization of sma-based aerostructures. *Smart Materials and Structures*, 20:094006, 2011.
- [48] Moré J J and Sorensen D C. Newton’s method. Technical report, Argonne National Lab., IL (USA), 1982.
- [49] Nocedal J and Wright S J. *Numerical optimization*. Springer-Verlag, 1999.
- [50] Qi H J, Nguyen T D, Castro F, Yakacki C M, and Shandas R. Finite deformation thermo-mechanical behavior of thermally induced shape memory polymers. *Journal of the Mechanics and Physics of Solids*, 56:1730–1751, 2008.
- [51] Qi H J, Nguyen T D, Castro F, Yakacki C M, and Shandas R. Finite deformation thermo-mechanical behavior of thermally induced shape memory polymers. *Journal of the Mechanics and Physics of Solids*, 56(5):1730–1751, 2008.
- [52] P. Jones and B. R. Spence. Spacecraft solar array technology trends. *Aerospace and Electronic Systems Magazine, IEEE*, 26(8):17–28, 2011.
- [53] Gross K. Mechanical characterization of shape memory polymers to assess candidacy as morphing aircraft skin. Master’s thesis, University of Pittsburgh, 2006.

- [54] Kuder I K, Arrieta A F, Raither W E, and Ermanni P. Variable stiffness material and structural concepts for morphing applications. *Progress in Aerospace Sciences*, 63:33–55, 2013.
- [55] Sun L and Huang W M. Mechanisms of the multi-shape memory effect and temperature memory effect in shape memory polymers. *Soft Matter*, 6:4403–4406, 2010.
- [56] Sun L and Huang W M. Mechanisms of the multi-shape memory effect and temperature memory effect in shape memory polymers. *Soft Matter*, 6(18):4403–4406, 2010.
- [57] Sun L, Huang W M, Wang C C, Zhao Y, Ding Z, and Purnawali H. Optimization of the shape memory effect in shape memory polymers. *Journal of Polymer Science Part A: Polymer Chemistry*, 49:3574–3581, 2011.
- [58] A. Lendlein, H. Jiang, O. Junger, and R. Langer. Light-induced shape-memory polymers. *Nature*, 434:879–882, 2005.
- [59] J. S. Leng, X. Lan, Y. J. Liu, and S. Y. Du. Shape-memory polymers and their composites: stimulus methods and applications. *Progress in Materials Science*, 56:1077–1135, 2011.
- [60] Ahmad M, Luo J K, Xu B, Purnawali H, King P J, and Chalker P. Synthesis and characterization of polyurethane-based shape-memory polymers for tailored tg around body temperature for medical applications. *Macromol Chemphysic*, 212:592–602, 2011.
- [61] Avriel M. *Nonlinear programming: analysis and methods*. Courier Dover Publications, 2012.
- [62] Boyerinas B M, Clark W W, Weiland L M, and Joshi S. Design and fabrication of a variable stiffness link for use in an unmanned air vehicle. In *Proc. of ASME 2009 Conf. on Smart Materials, Adaptive Structures and Intelligent Systems*, volume 2, pages 317–323, 2009.
- [63] Chen M, Tsai H, Chang Y, Lai W, Mi F, Liu C, Wong H, and Sung H. Rapidly self-expandable polymeric stents with a shape-memory property. *Biomacromolecules*, 8:2774–2780, 2007.
- [64] Chen M, Tsai H, Chang Y, Lai W, Mi F, Liu C, Wong H, and Sung H. Rapidly self-expandable polymeric stents with a shape-memory property. *Biomacromolecules*, 8:2774–2780, 2007.
- [65] DiOrio A M, Luo X F, Lee K M, and Mather P T. A functionally graded shape memory polymer. *Soft Matter*, 7:68–74, 2011.
- [66] Ecker M and Pretsch T. Durability of switchable qr code carriers under hydrolytic and photolytic conditions. *Smart Materials and Structures*, 22(9):094005, 2013.

- [67] Ecker M and Pretsch T. Multifunctional poly (ester urethane) laminates with encoded information. *RSC Advances*, 4(1):286–292, 2014.
- [68] Freund R M and Mizuno S. Interior point methods: current status and future directions. *Optima*, 51:1–9, 1996.
- [69] Huang W M. Novel applications and future of shape-memory-polymers. *CRC Press*, 2010.
- [70] Langelaar M and Keulen K V. Sensitivity analysis of shape memory alloy shells. *Computer and Structures*, 86:964–976, 2008.
- [71] Langelaar M and Keulen K V. Sensitivity analysis of shape memory alloy shells. *Computer and Structures*, 86:964–976, 2008.
- [72] Mitchell M. *An introduction to genetic algorithms*. MIT Press, 1998.
- [73] Pitt D M, Dunne J P, and White E V. Sampson smart inlet design overview and wind tunnel test: part 1. design overview. In *Proc. SPIE*, volume 4698, page 13, 2002.
- [74] Pitt D M, Dunne J P, and White E V. Sampson smart inlet design overview and wind tunnel test: part 2. wind tunnel test. In *Proc. SPIE*, volume 4698, page 24, 2002.
- [75] Wache H M, Tartakowska D J, and Hentrich A. Development of a polymer stent with shape memory effect as a drug delivery system. *Journal of Materials Science: Materials in Medicine*, 14:109–112, 2003.
- [76] J. Manzo and E. Garcia. Demonstration of an in situ morphing hyperelliptical cambered span wing mechanism. *Smart Materials and Structures*, 19(2):025012, 2010.
- [77] MATLAB. <http://www.mathworks.com/products/matlab>.
- [78] Amber JW McClung, Gyaneshwar P Tandon, and Jeffery W Baur. Strain rate-and temperature-dependent tensile properties of an epoxy-based, thermosetting, shape memory polymer (veriflex-e). *Mechanics of Time-Dependent Materials*, 16(2):205–221, 2012.
- [79] A. Meguro, K. Shintate, M. Usui, and A. Tsujihata. In-orbit deployment characteristics of large deployable antenna reflector onboard engineering test satellite viii. *Acta Astronautica*, 65(9):1306–1316, 2009.
- [80] Qinghao Meng and Jinlian Hu. A review of shape memory polymer composites and blends. *Composites Part A: Applied Science and Manufacturing*, 40(11):1661–1672, 2009.
- [81] M. Mitchell. *An introduction to genetic algorithms*. MIT Press, 1998.

- [82] Kudva J N. Overview of the darpa smart wing project. *Journal of Intelligent Materials Systems and Structures*, 15:261–267, 2004.
- [83] G. Farkas N. Friedman and A. Ibrahimbegovic. Deployable/retractable structures towards sustainable development. *Pollack Periodica*, 6:85–97, 2011.
- [84] K. Nagaya and H. Ryu. Deflection shape control of a flexible beam by using shape memory alloy wires under the genetic algorithm control. *Journal of Intelligent Material Systems and Structures*, 7:336–341, 1996.
- [85] O. E. Ozbulut and S. Hurlebaus. Evaluation of the performance of a sliding-type base isolation system with a niti shapememoryalloy device considering temperature effects. *Engineering Structures*, 32:238–249, 2010.
- [86] Armand P, Gilbert J C, and Jan-Jégou S. A feasible bfgs interior point algorithm for solving convex minimization problems. *SIAM Journal on Optimization*, 11(1):199–222, 2000.
- [87] A. Pagano, S. Ameduri, V. Cokonaj, A. Prachar, Z. Zachariadis, and D. Drikakis. Helicopter blade twist control through sma technology: optimal shape prediction, twist actuator realisations and main rotor enhanced performance computation. In *Proceedings of 35th European Rotorcraft Forum*, volume 22, page 25, 2009.
- [88] D. M. Pitt, J. P. Dunne, and E. V. White. Sampson smart inlet design overview and wind tunnel test: part i. design overview. In *Proc. SPIE*, pages 13–23, 2002.
- [89] D. M. Pitt, J. P. Dunne, and E. V. White. Sampson smart inlet design overview and wind tunnel test: part ii. wind tunnel test. In *Proc. SPIE*, pages 24–36, 2002.
- [90] J. Reddy. *An Introduction to the finite element method*. McGraw-Hill, 2005.
- [91] Hayashi S, Tasaka Y, Hayashi N, and Akita Y. Development of smart polymer materials and its various applications. *Review Literature And Arts Of The Americas*, 41:1–3, 2004.
- [92] Reese S, Bol M, and Christ D. Finite element-based multi-phase modelling of shape memory polymer stents. *Computer Methods in Applied Mechanics and Engineering*, 199:1276–1286, 2010.
- [93] Wang S and Brigham J C. A computational inverse problem approach for the design of morphing processes in thermally activated smart structural materials. In *SPIE Smart Structures and Materials+ Nondestructive Evaluation and Health Monitoring*, pages 79771N–79771N. International Society for Optics and Photonics, 2011.
- [94] Wang S and Brigham J C. A computational framework for the optimal design of morphing processes in locally activated smart material structures. *Smart Materials and Structures*, 21, 2012.

- [95] Wang S and Brigham J C. An adjoint based approach for optimal design of morphing smp. In *ASME 2013 Conference on Smart Materials, Adaptive Structures and Intelligent Systems*, pages V002T06A024–V002T06A024. American Society of Mechanical Engineers, 2013.
- [96] SIMULIA. <http://www.simulia.com>.
- [97] D. Smith, A. Isikveren, R. Ajaj, and M. Friswell. Multidisciplinary design optimization of an active nonplanar polymorphing wing. In *27th International Congress of The Aeronautical Sciences (ICAS)*, 2010.
- [98] A. Y. Sofla, D. M. Elzey, and H. N. Wadley. Two-way antagonistic shape actuation based on the one-way shape memory effect. *Journal of Intelligent Material Systems and Structures*, 19(9):1017–1027, 2008.
- [99] F. K. Straub, V. R. Anand, T. S. Birchette, and B. H. Lau. Smart rotor development and wind tunnel test. Technical report, DTIC Document, 2009.
- [100] J. K. Strelec, D. C. Lagoudas, M. A. Khan, and J. Yen. Design and implementation of a shape memory alloy actuated reconfigurable airfoil. *Journal of Intelligent Material Systems and Structures*, 14:257–273, 2003.
- [101] J. K. Strelec, D. C. Lagoudas, M. A. Khan, and J. Yen. Design and implementation of a shape memory alloy actuated reconfigurable airfoil. *Journal of Intelligent Material Systems and Structures*, 14:257–273, 2003.
- [102] L. Sun, W. M. Huang, Z. Ding, Y. Zhao, C. C. Wang, H. Purnawali, and C. Tang. Stimulus-responsive shape memory materials: a review. *Materials and Design*, 33:577–640, 2012.
- [103] Xie T and Rousseau I A. Facile tailoring of thermal transition temperatures of epoxy shape memory polymers. *Polymer*, 50:1852–1856, 2009.
- [104] J. Tyner, M. Coates, D. Holloway, K. Goldsmith, C. Daniels, T. Vranicar, J. Roling, D. Jensen, A. Mundy, and L. B. Peterson. The design of a portable and deployable solar energy system for deployed military applications. In *Systems and Information Engineering Design Symposium (SIEDS), 2011 IEEE*, pages 50–53, 2011.
- [105] Srivastava V, Chester S A, and Anand L. Thermally actuated shape-memory polymers: experiments, theory, and numerical simulations. *Journal of the Mechanics and Physics of Solids*, 58:1100–1124, 2010.
- [106] R. Vos, R. Barrett, and D. Zehr. Magnification of work output in pbp class actuators using buckling/converse buckling techniques. In *Proceedings of the 49th AIAA/ASME/ASCE/AHS/ASC Structures, Structural Dynamics and Materials Conference*, pages 2008–1705, 2008.

- [107] Aquino W and Brigham J C. *Computational inverse problem techniques in vibroacoustics*. Chapter 4 in Biomedical applications of vibration and acoustics for imaging, characterization, and diagnostics. ASME, 2008.
- [108] Clark W W, Brigham J C, Mo C, and Joshi S. Modeling of a high-deformation shape memory polymer locking link. In *Proc. SPIE*, volume 7645, 2010.
- [109] Paquette J W and Kim K J. Ionomeric electroactive polymer artificial muscle for naval applications. *Oceanic Engineering, IEEE*, 29(3):729–737, 2004.
- [110] H. M. Wache, D. J. Tartakowska, and A. Hentrich. Development of a polymer stent with shape memory effect as a drug delivery system. *Journal of Materials Science: Materials in Medicine*, 14:109–112, 2003.
- [111] Lan X, Liu Y, Lv H, Wang X, Leng J, and Du S. Fiber reinforced shape-memory polymer composite and its application in a deployable hinge. *Smart Materials and Structures*, 18:024002, 2009.
- [112] Bar-Cohen Y. Electroactive polymers: current capabilities and challenges. In *SPIE's 9th Annual International Symposium on Smart Structures and Materials*, pages 1–7, 2002.
- [113] Du H Y and Zhang J H. Solvent induced shape recovery of shape memory polymer based on chemically cross-linked poly(vinyl alcohol). *Soft Matter*, 6:3370–3376, 2010.
- [114] Jarny Y, Ozisik M N, and Bardon J P. A general optimization method using adjoint equation for solving multidimensional inverse heat conduction. *International Journal of Heat and Mass Transfer*, 34:2911–2919, 1991.
- [115] W. Yin, T. Fu, Y. Liu, and J. Leng. Structural shape sensing for variable camber wing using fbg sensors. In *the 16th International Symposium on: Smart Structures and Materials Nondestructive Evaluation and Health Monitoring*, 2009.
- [116] A. Yousefi-Koma and D. G. Zimicik. Applications of smart structures to aircraft for performance enhancement. *Canadian Aeronautics and Space Journal*, 49:163–172, 2003.
- [117] K. Yu, W. Yin, S. Sun, Y. Liu, and J. Leng. Design and analysis of morphing wing based on smp composite. In *the 16th International Symposium on: Smart Structures and Materials Nondestructive Evaluation and Health Monitoring*, 2009.
- [118] Wei Z, Sandstrom R, and Miyazaki S. Shape-memory materials and hybrid composites for smart systems: part i shape-memory materials. *Journal of Materials Science*, 33(15):3743–3762, 1998.